NAL TR-685T

ISSN 0389-4010
UDC 629. 735. 014. 16 :
629. 7. 025. 35 :
534. 2

TECHNICAL REPORT OF NATIONAL AEROSPACE LABORATORY

TR-685T

Aerodynamic Noise Generated by Jet-Wing/Flap Interactions of the External USB Configuration of STOL Aircraft

[I] 8% — Scale Cold-Flow Model Analysis

Masataka MAITA and Shigemi SHINDO

OCTOBER, 1981

NATIONAL AEROSPACE LABORATORY

CHŌFU, TOKYO, JAPAN

Aerodynamic Noise Generated by Jet-Wing/Flap Interactions of the External USB Configuration of STOL Aircraft [I] 8%-Scale Cold-Flow Model Analysis

Masataka MAITA* and Shigemi SHINDO**

ABSTRACT

The acoustic characteristics of the external upper surface blowing (USB) concept of a powered high lift system (PHLS) were studied experimentally using an 8%-scale static cold flow model. Observations of exhaust jet flow attachment and spreading characteristics on wing/flap surface were also carried out using several flow visualization techniques.

Noise reduction data were obtained by optimizing basic jet nozzle-wing/flap structural geometries for the lowest noise. Among the associated parameters which define USB-PHLS configurations, (I) the location relative to wing/flap and the shape of the exhaust jet nozzle and (II) flow attachment devices are important parameters. Flow characteristics dependence on these parameters and PHLS noise were also obtained.

From far-field noise spectra, OASPL dependence on jet velocity and coherence across near-field surface pressure, it was concluded that the flap trailing edge noise was the most predominant noise source. Several acoustically treated flaps and serrated trailing edge design techniques were applied to attenuate edge noise.

概　　要

外部上面吹出し（ＵＳＢ）方式は，短距離離着陸（ＳＴＯＬ）機の高揚力システムに於ける有力な方法の一つであるが，これは推進用ターボファンエンジンの排気を，その下流に装備した翼／フラップの上面にそって吹き出して下方に偏向し，低速時の揚力の増加を得るものである。騒音問題から言うと，これに因り一般のＣＴＯＬ機には生じて居ない排気ジェットと翼／フラップとの干渉による高揚力システムからの新たな騒音発生をもたらす。今後の騒音規制に適合する騒音低減化技術の確立のためには，高揚力システムからの騒音特性を把握し，その騒音発生及び伝播メカニズムを解明することが重要課題である。これらは複雑なメカニズムを呈して居り，正確な理論的予測を困難にしているが，本研究に於いては，USB方式高揚力システムの８％スケールモデルを用いて，実験的にその騒音特性を明らかにした。

* Noise and Emission Research Group, 4th Group.
** Noise and Emission Research Group, 1st Group.

又ＵＳＢ方式高揚力システムからの騒音が，翼面上の排気ジェット流の特性に関連し，従ってこれを決定付ける高揚力システムの幾可形状に依存することを示し，排気流れの可視化を行ない，排気ジェット特性パラメーター$\alpha_{s.p.}$を新しく定義，導入し，乱れのレベル及び騒音レベルとの定量的な関係を明らかにした。

これらの基礎データをもとに，ＵＳＢ方式高揚力システムの低騒音への最適化及び騒音低減化のための基本的概念を示し，これら低減化方法の評価を行なった。

Nomenclature

AR	Aspect ratio defined as the square of Nozzle width L divided by nozzle area, L^2/Area.
AR_e	Aspect ratio defined as nozzle area divided by the square of nozzle height h, Area/h^2.
U_{jet}	The mean jet velocity at USB nozzle exit.
St	Strouhal number based upon the wall jet thickness at the flap trailing edge, δ.
$\alpha_{s.p.}$	The Jet Flow Spreading Parameter defined in Figure 16 of Chapter VI.
PHLS-OASPL	Overall sound pressure level at the direction below the wing, radiated from a powered high lift system.
U_{sb}	Mean velocity of secondary air blowing from a flap trailing edge slit.
δ_f	The flap deflection angle, [deg.]
f_{peak}	The frequency corresponding to the maximum SPL in acoustic spectrum.

INTRODUCTION

The external upper surface blowing [USB] is one of the primary concepts in achieving powered lift for short takeoff and landing [STOL] aircraft applications. The powered lift augmentation during low speed STOL operations is derived by deflecting turbofan engine exhaust jet downward adjacent to the wing and flap upper surface by Coanda effect.

From the acoustic view point, this design concept produces additional noise as jet exhaust flow interacts with the wing/flap surfaces. From the morphology of past studies, the resulting STOL aircraft noise sources would be qualitatively categorized as the schematics of Figure 1. In order to meet the stringent noise level goals which are being put forth and community acceptance, noise reduction techniques must be developed. Among the noise associated with USB-STOL aircraft powered by turbofan engines, noise from turbofan engine and USB Powered high lift system are major contributive factors. Engine noise problems are common to those of conventional [CTOL] aircraft, and during the past decade, researches on noise reduction technology were primarily directed at engine noise sources. By the development of acoustical treated engine nacelle, engine noise dominated by fan-generated noise was progressively reduced. Noise generated by powered high lift system is peculiar to STOL aircraft. While the stage of art of this subject is advancing, the details of the actual noise-

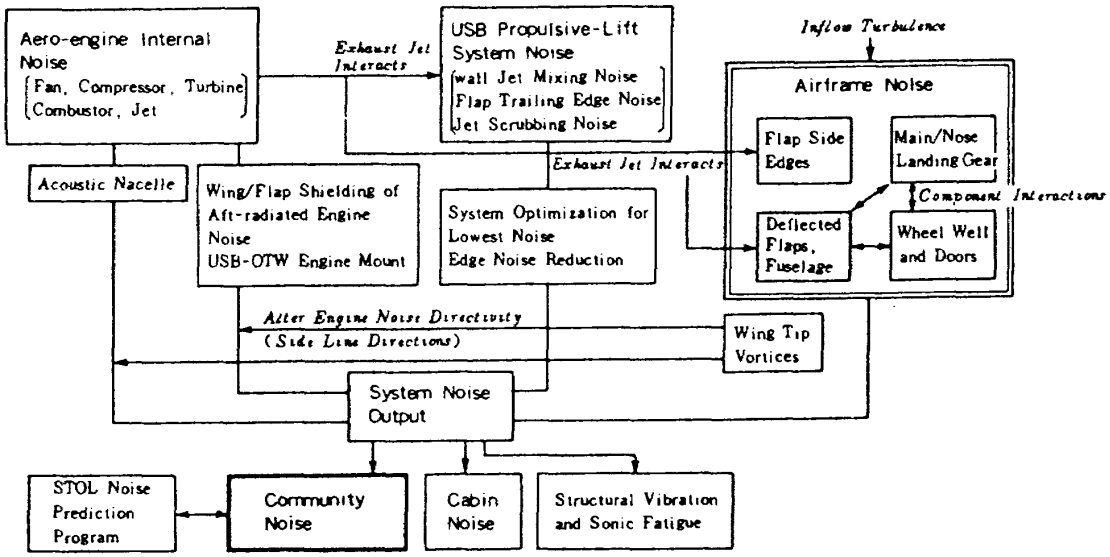

Figure 1 STOL Aircraft Noise

generation and radiation mechanisms are not yet known.

For this purpose, a noise program was carried out experimentally to obtain extensive USB powered high lift system [USB-PHLS] noise data, comparing with the visualization of exhaust jet flow characteristics over the wing and flap surfaces by 8%-scale static model configurations.

In the present paper, we attempt to summarize the main results and conclusions concerning the following properties.

[1] Noise characteristics of the external upper surface blowing powered high lift system.

[2] The identification of the most predominant noise source.

[3] USB-PHLS noise dependence on exhaust jet flow characteristics relating to the noise generation mechanisms.

[4] The optimization of USB-PHLS configuration for the lowest noise.

[5] The attenuation of the predominant noise by applying several noise reduction techniques.

When discussing the noise reduction and optimization data, we restrict ourselves mainly to the aeroacoustic characteristics radiating to the direction below the wing and flap because the noise radiated above the wing is of little importance from a community noise point of view.

APPARATUS AND PROCEDURE

The typical setup of the basic model configuration for the noise experiments in an anechoic room is shown in Photograph 1. This 8%-scale upper surface blowing cold flow model, as illustrated in Figure 2, consists of a jet blowing over the main wing and USB flaps assembly surface, simulating the typical USB-PHLS system configuration by choosing any of the variable parameters as shown in Figures 3 and 4. The USB flaps are of fore/main double-flap type and the cross sections of δ_f=0° (clean), 10°, 20°, 30° and 60° flap configurations are presented in Figure 5. The engine exhaust was simulated by an air jet and its mean velocities at the nozzle exit were calcu-

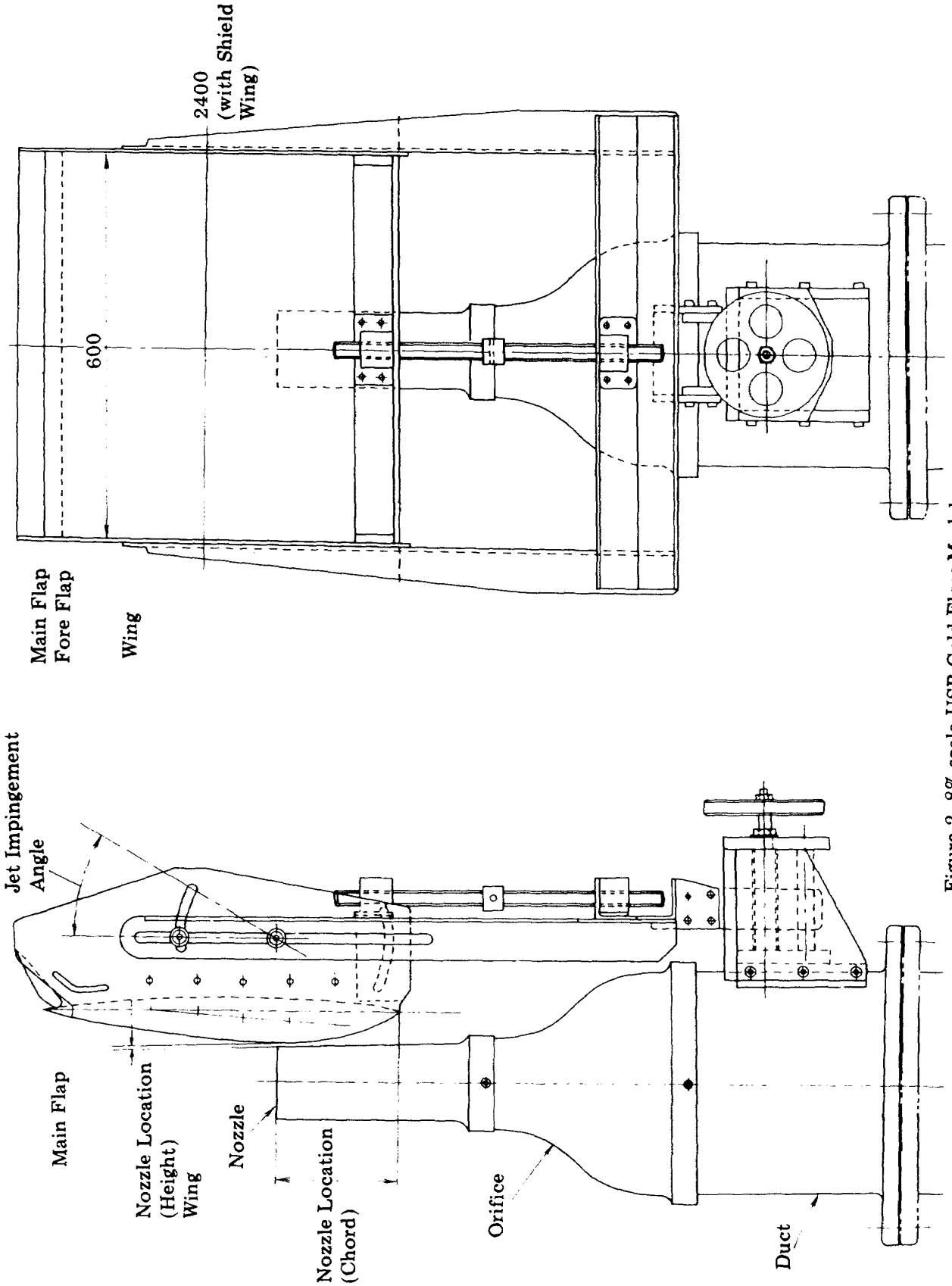

Figure 2 8%-scale USB Cold Flow Model

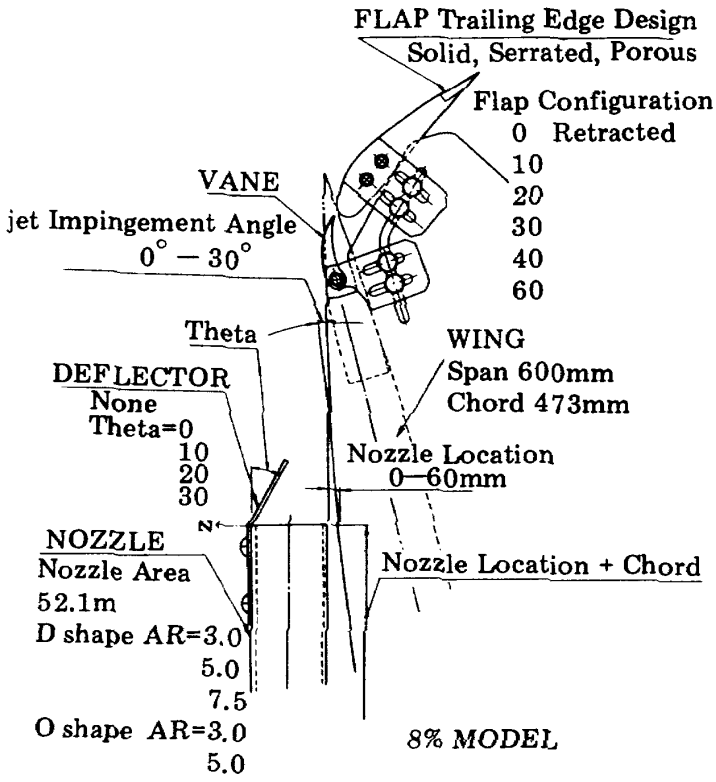

Figure 3 Parameters defining USB-PHLD system configurations

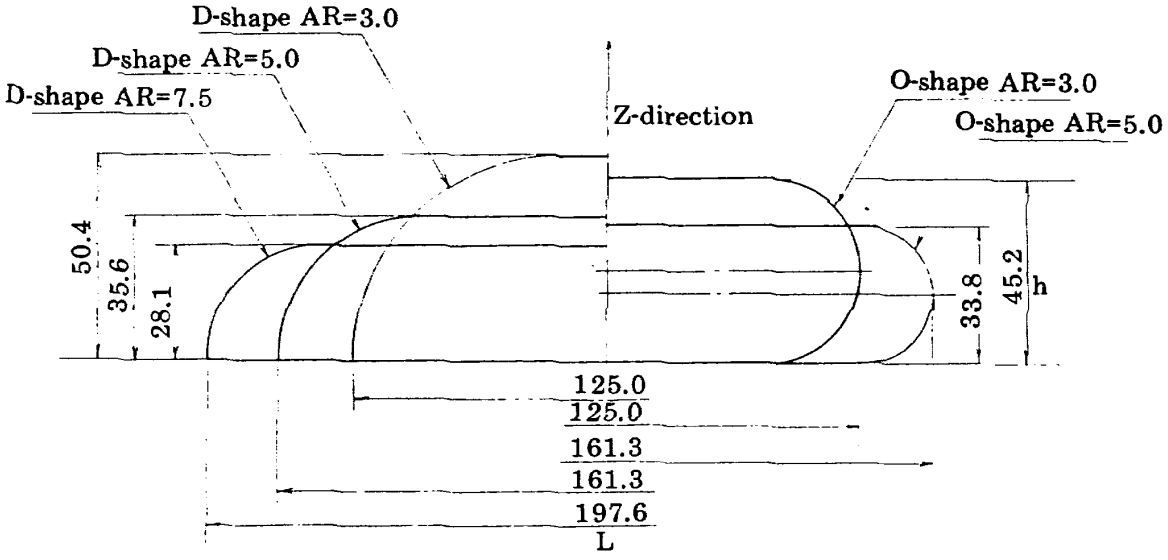

Symbol	D-shape Nozzle			O-shape Hozzle	
	D-3.0	D-5.0	D-7.5	0-3.0	0-5.0
AR_e=Area/h^2	2.05	4.11	6.60	2.55	4.56
AR=L^2/Area	3.00	4.99	7.45	3.00	4.99

Figure 4 USB Nozzle exit geometries

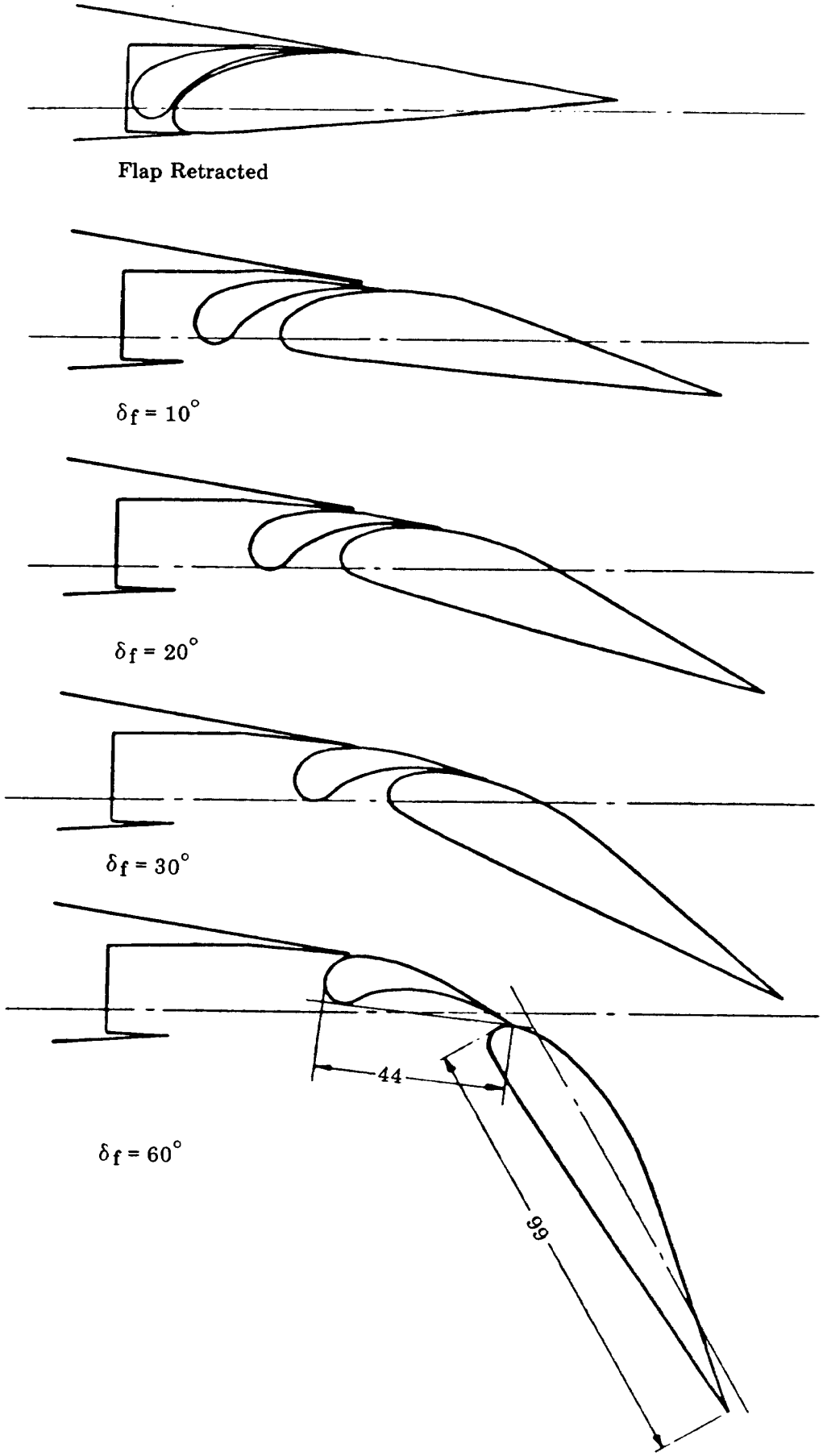

Figure 5 USB flap configurations

Photograph 1 Typical setup of basic model in an anechoic room

lated from the plenum tempeature, pressure and ambient conditions.

Far-field noise data were taken for all parameter variations by one-half inch condenser microphones placed on an 2.5-meter radius centered at the jet nozzle exit. The locations of far-field microphones for taking Flyover and Sideline noise are presented in Figure 6.

Near-field fluctuating surface pressure was measured by probe microphones installed at the wing surface to determine noise coherence between the near-field and the far-field. Photograph 2 shows the probe microphones which are mounted flush on the main flap upper surface, as these examples.

Noise data were FM recorded on a multi-channel Data Recorder at tape speed of 30ips. A schematic diagram of data acquisition and reduction systems is shown in Figure 7.

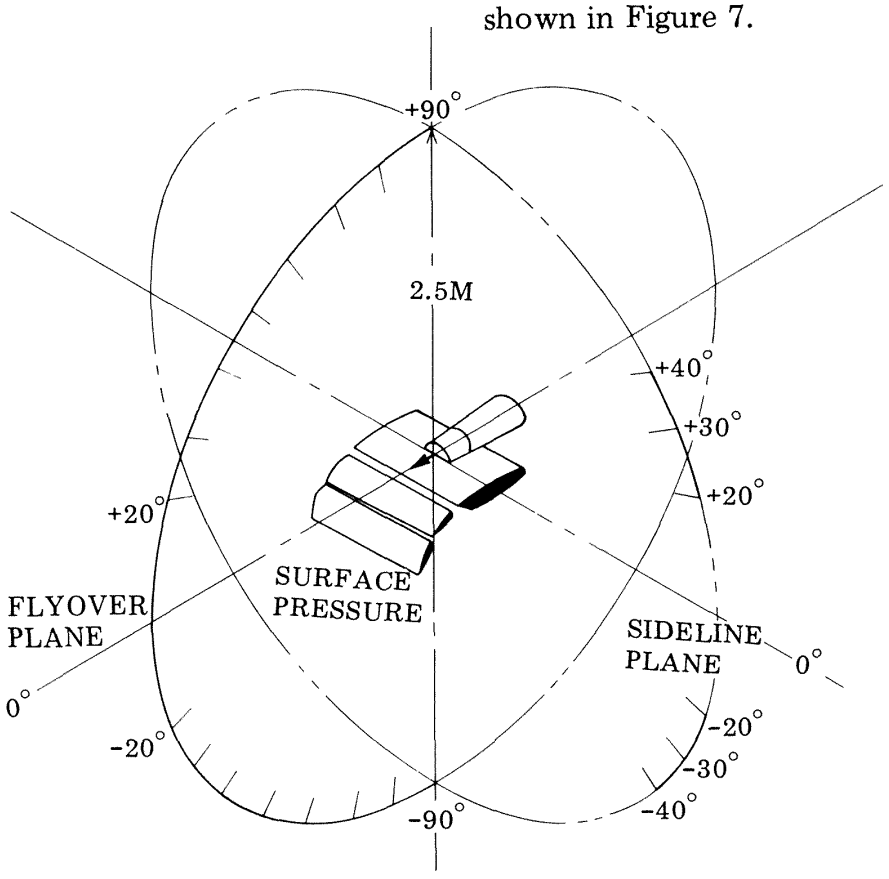

Figure 6 Far-field microphone locations

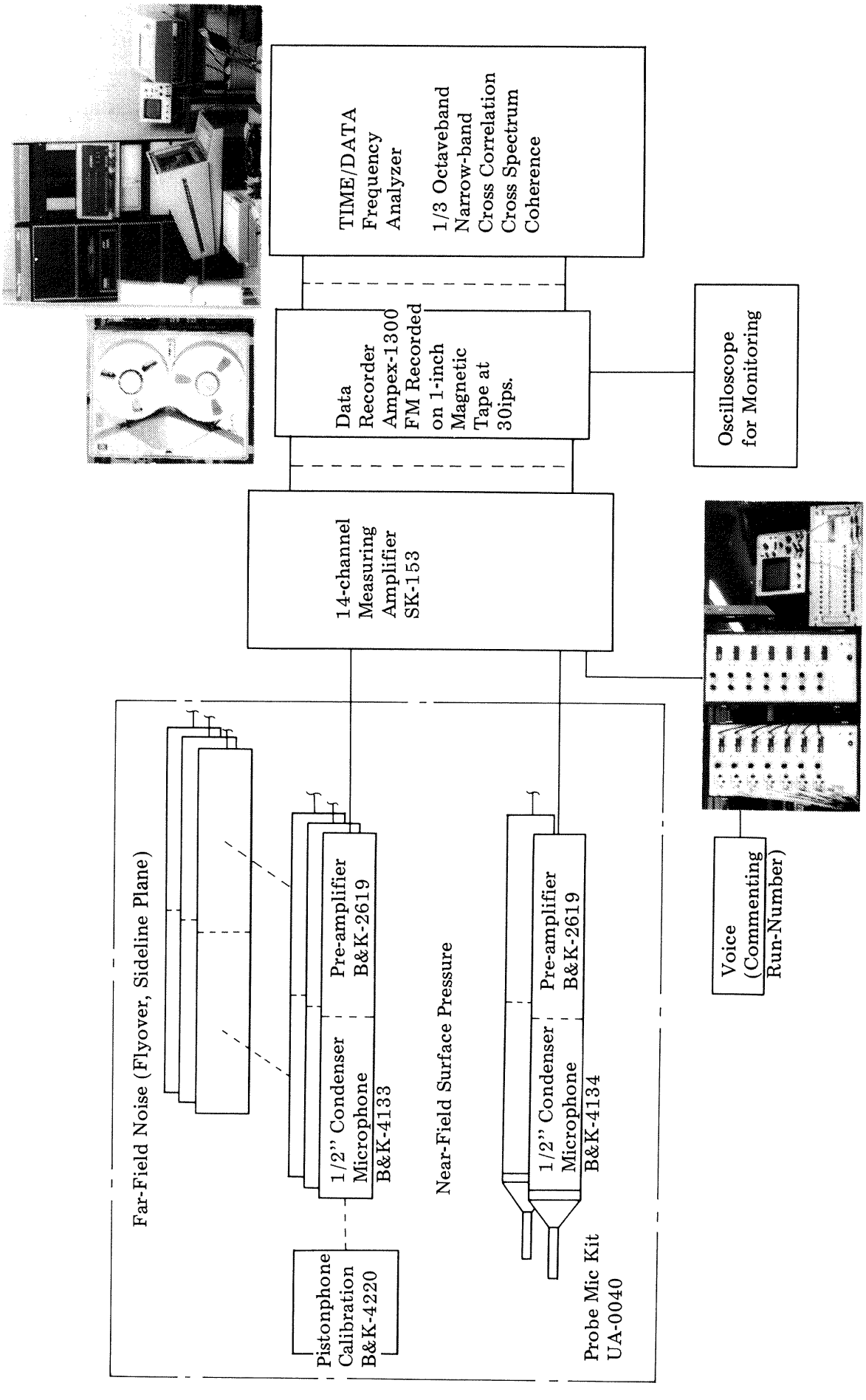

Figure 7 A Schematic Diagram of data acquisition and reduction

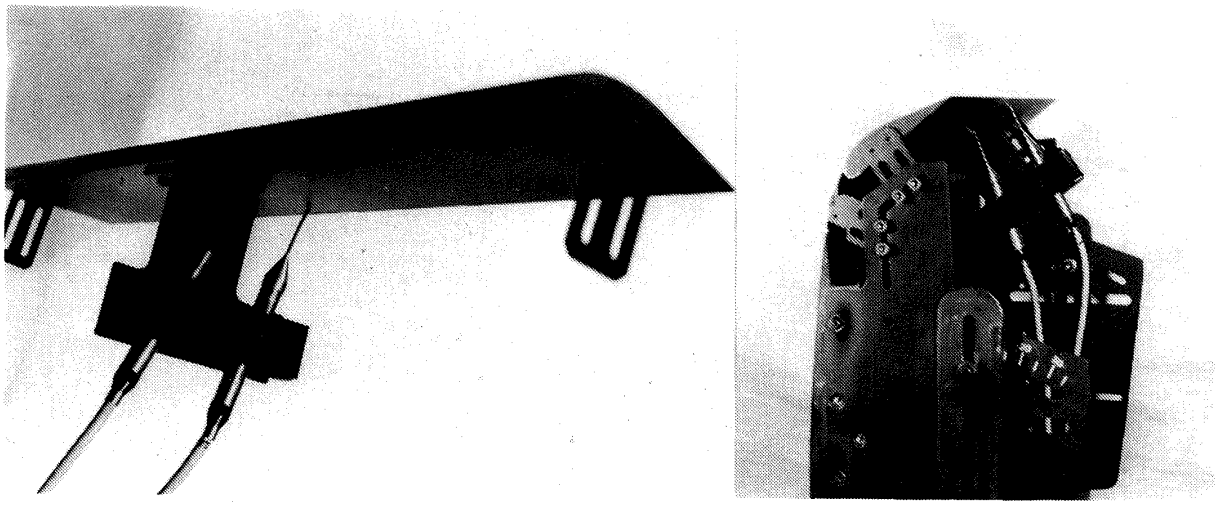

Photograph 2 Probe microphones installed at the main flap

Jet flow behaviour over the wing/flap surface was visualized by several flow visualization techniques such as Oil flow, the Liquid Crystals and Schlieren Photographs, to determine how USB-PHLS system configurations affect exhaust jet flow spreading and attachment characteristics by changing design parameters.

RESULTS AND DISCUSSIONS

The effect of jet velocity variation on USB-PHLS noise sound pressure level for the typical system configuration, as an example, is shown in Figure 8. (PHLS system parameters chosen are commented on each Figure.), while the jet nozzle alone as a component case is shown in Figure 9.

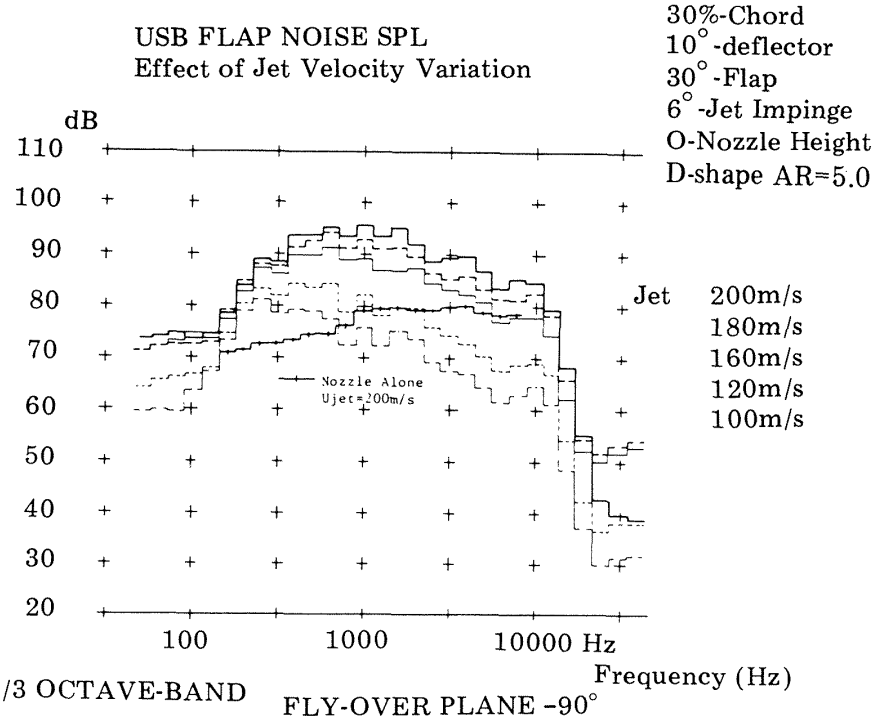

Figure 8 The effect of jet velocing variation on USB-PHLS noise spectra a at the direction below the wing (Flyover -90)

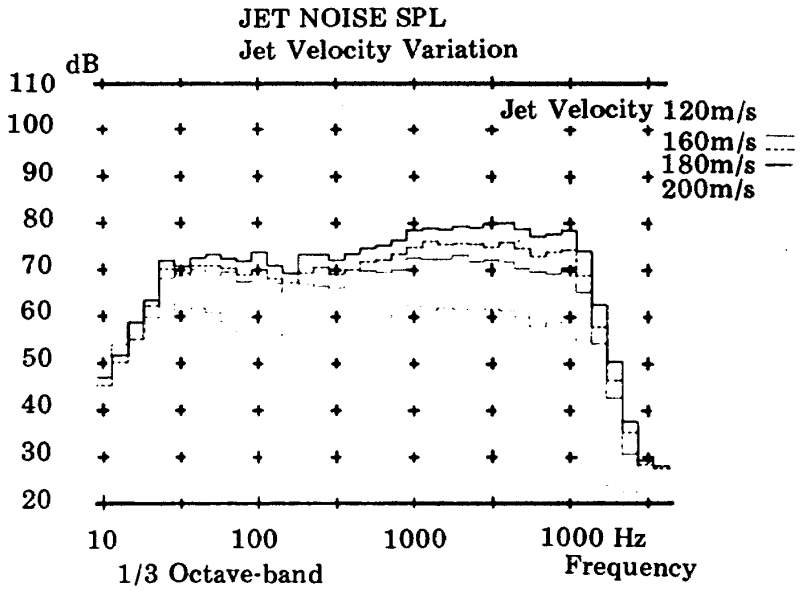

Figure 9 The effect of jet velocity variation on jet noise (Jet nozzle alone component case) at the direction below the wing (Flyover -90°)

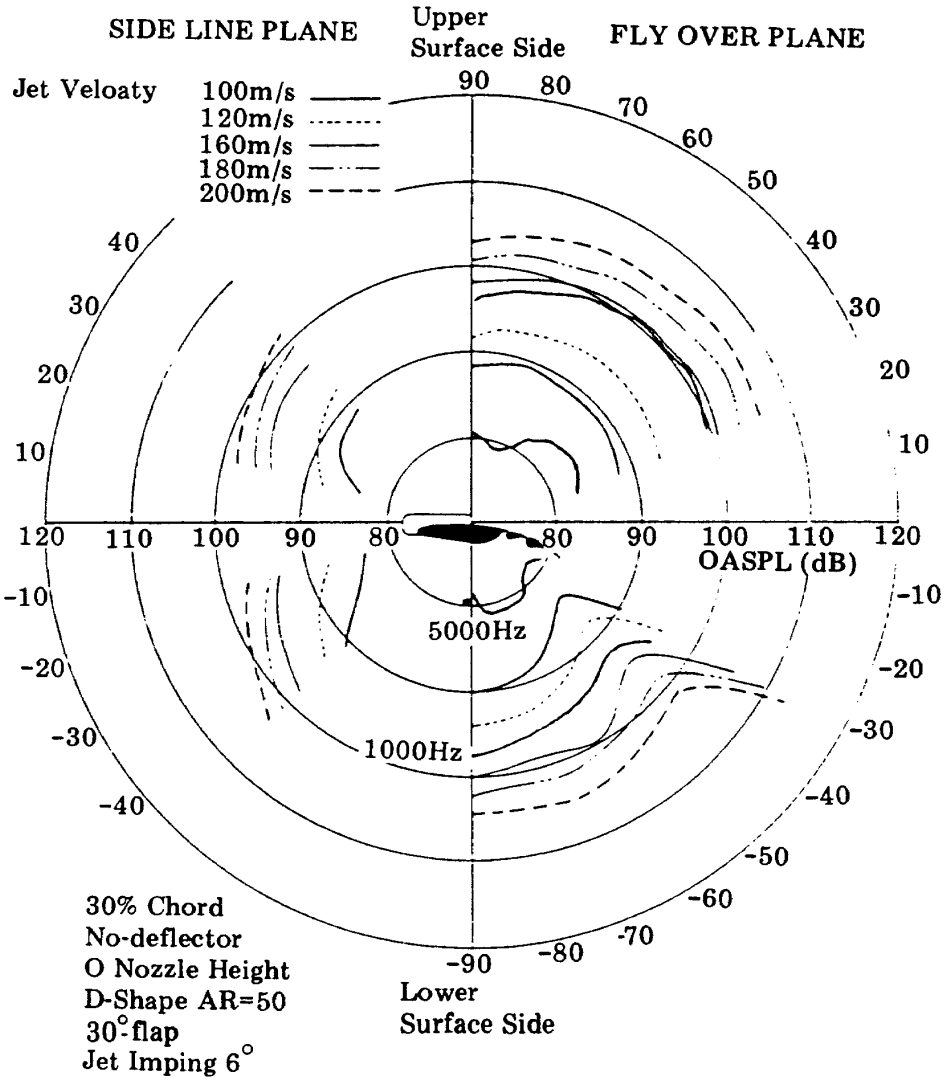

Figure 10 USR-PHLS noise directivity patterns and the effect of exhaust jet velocity variations

The directivity patterns of overall sound pressure level (OASPL) and selected 1/3 octave-band sound intensities (1000Hz and 5000Hz) are shown in Figure 10, indicating that the velocity exponents of sound radiated from USB-PHLS is a function of direction. OASPL for the jet alone case varies with its exhaust velocity according to Lighthill's 8th-power law dependence as shown in Figure 11. The overall sound intensity from USB-PHLS configuration varies as $U_{jet}^{5.1}$—$U_{jet}^{5.9}$ depending on the direction (Figure 12 is an example at Flyover Plane ±60° directions), though the sound intensity at 1/3 octave band center frequency 5000Hz where jet mixing noise is thought to be contributive, varies as U_{jet}^{8} approximately at constant.

Acoustic spectra from USB-PHLS in the high-frequency ranges (above 3000Hz) are very similar to jet-alone noise spectra. Figure 13 shows the relative sound pressure level (SPL) being jet nozzle alone noise as baseline, where its peak relative noise level frequency corresponds to the peak level frequency of USB-PHLS noise.

Of the noise field associated with USB-PHLS system as categorized in the previous section, the important problem is which noise generating mechanism is the most predominant. In Figure 14, the comparison of noise spectra from USB-PHLS (retracted flap) in the directions perpendicular to the flap trailing edge

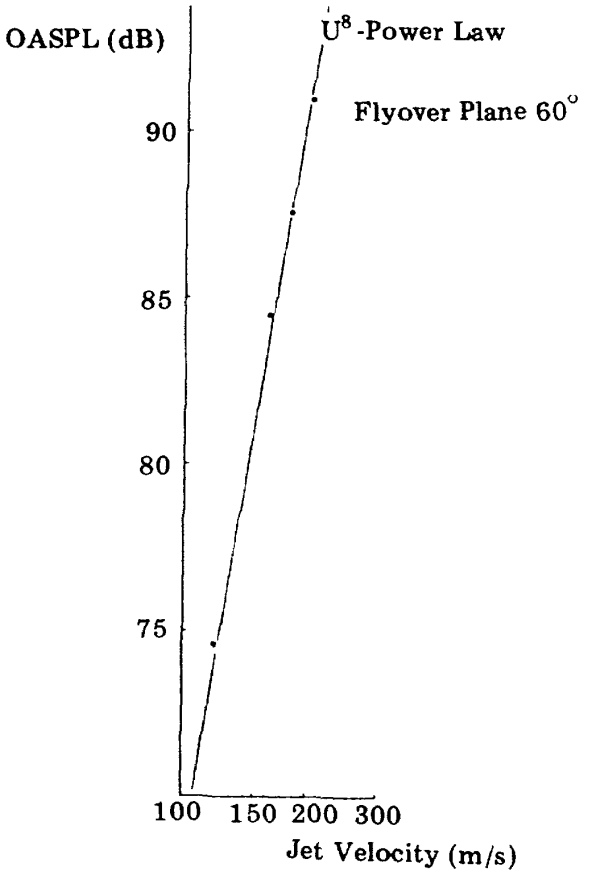

Figure 11 Overall Sound Pressure Level of jet alone case dependence on jet velocity

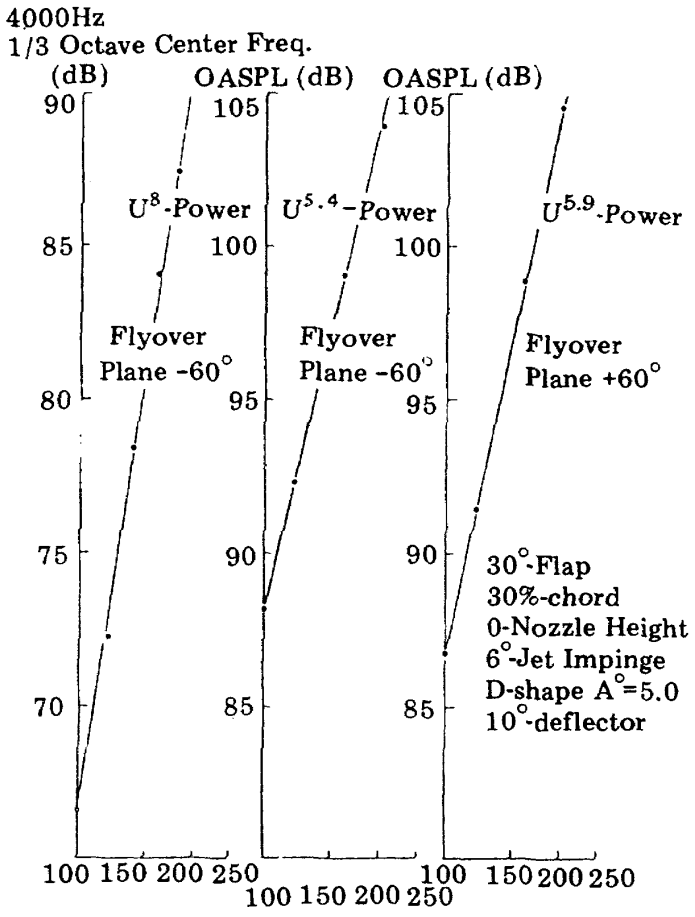

Figure 12 OASPL dependence of USB-PHLS noise on jet velocity

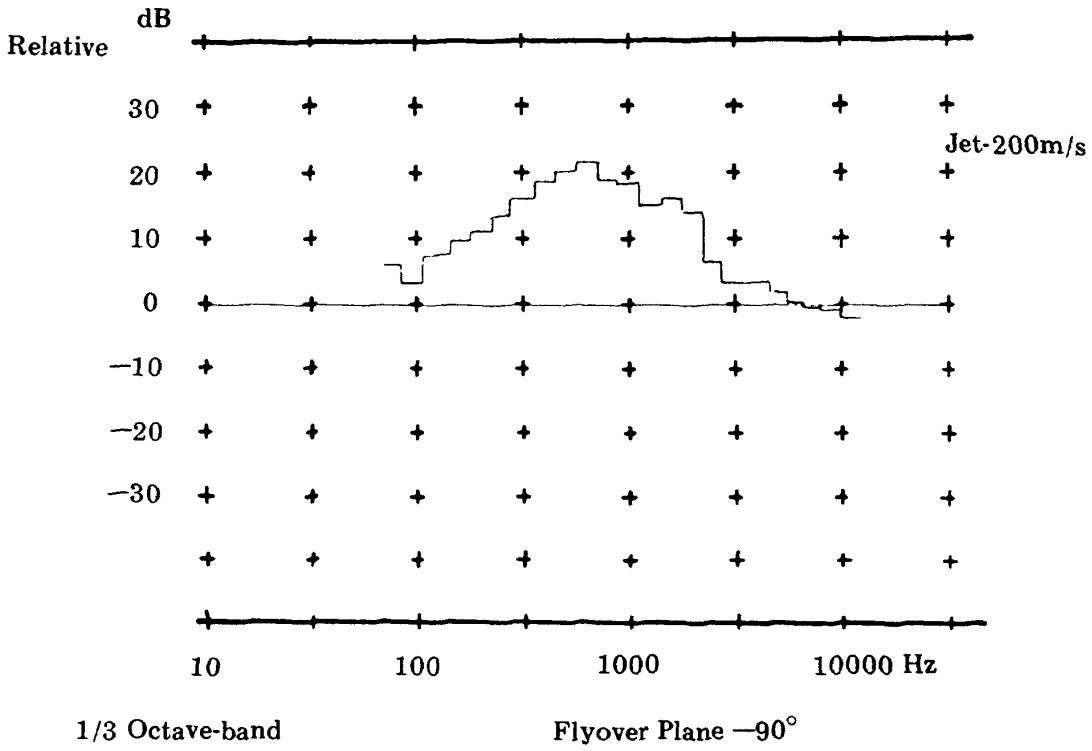

Figure 13 USB-PHLS relative noise SPL spectra as jet alone noise being baseline

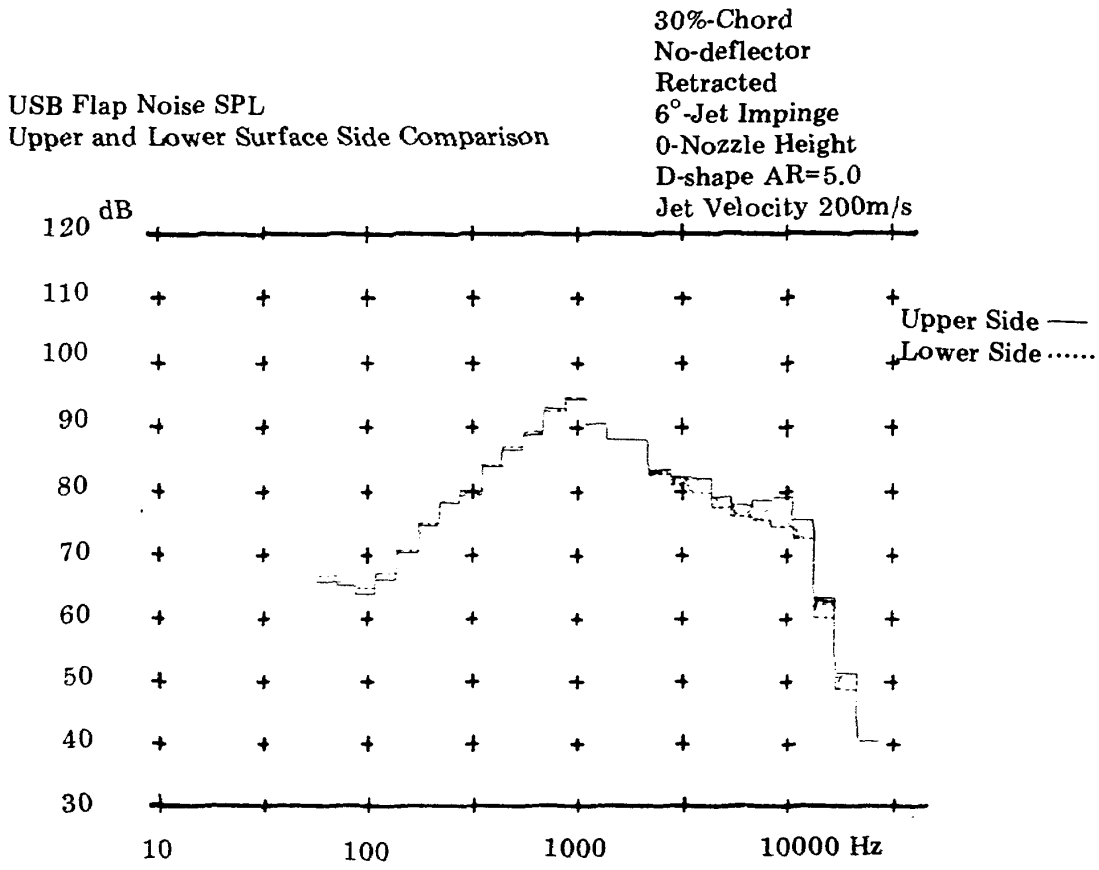

Figure 14 Comparison of 1/3 Octave-band spectra of USB-PHLS noise in the directions perpendicular to flap trailing edge

below and above the wing/flap (lower and upper parts of Fig. 14 respectively) is shown. In the high-frequency ranges, the sound levels below the wing are less than the levels above the wing due to the shielding/reflective effect by the wing/flap. From these results, it can be concluded that the high-frequency noise in the spectra is primary contributed by the jet mixing process (jet and wall jet mixing).

In the spectra of Figure 14, both peak level frequencies lie in the same frequency ranges and its sound intensities are of the same order of magnitude. It can be postulated that the above results are possible when the predominant noise source contributing to the peak sound intensity level frequency ranges is located near the flap trailing edge where the least noise shielding by the wing/flap occurs.

Figure 15 shows the normalized SPL spectral density using Strouhal number based upon the wall jet thickness δ at the flap trailing edge, where δ was estimated by conferring Reddy et.al.[1] Brown[2], and Tam's[3] experimental data and found to be approximately 30% of the USB nozzle exit height and noise intensity dependence on 5th-power law of the jet exhaust velocity.

Strouhal number corresponding to spectral peak level frequency ranges is approximately constant at 0.05 for all cases, and normalized SPL spectral densities have the similarity in form in the peak level frequency ranges and scatter outside these ranges.

A series of coherence data between the near-field fluctuating surface pressure and the far-field sound were taken. For examples, Figures 16 and 17 show coherence across the flap trailing edge when the jet velocity is 200m/s and 120m/s respectively.

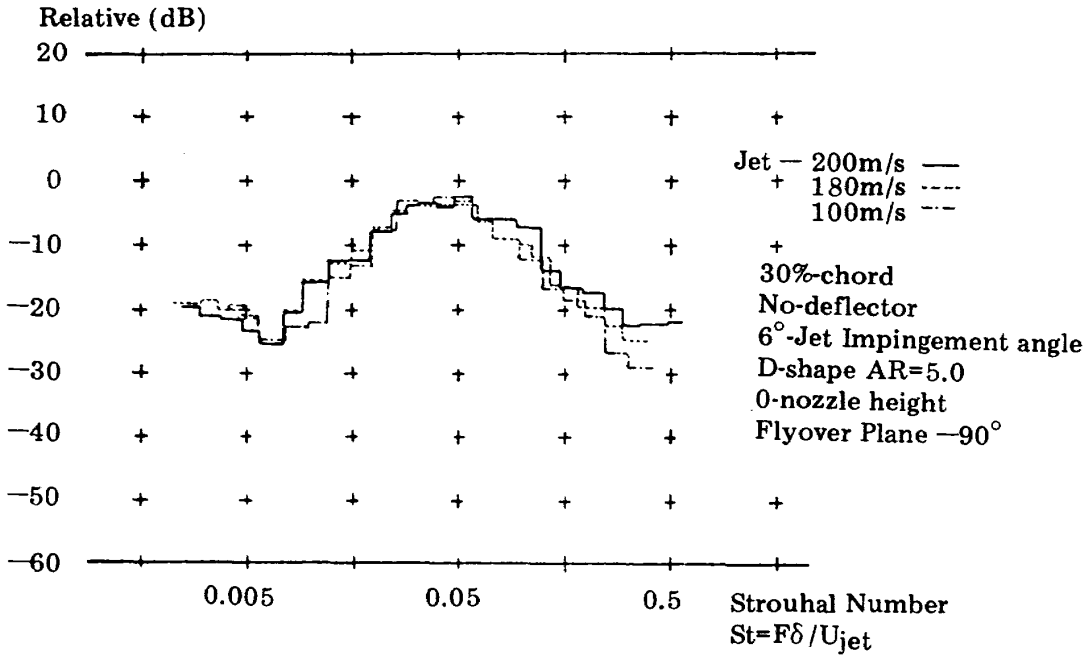

Figure 15 The normalized SPL spectral density using Strouhal number based upon the wall jet thickness at the flap trailing edge, δ

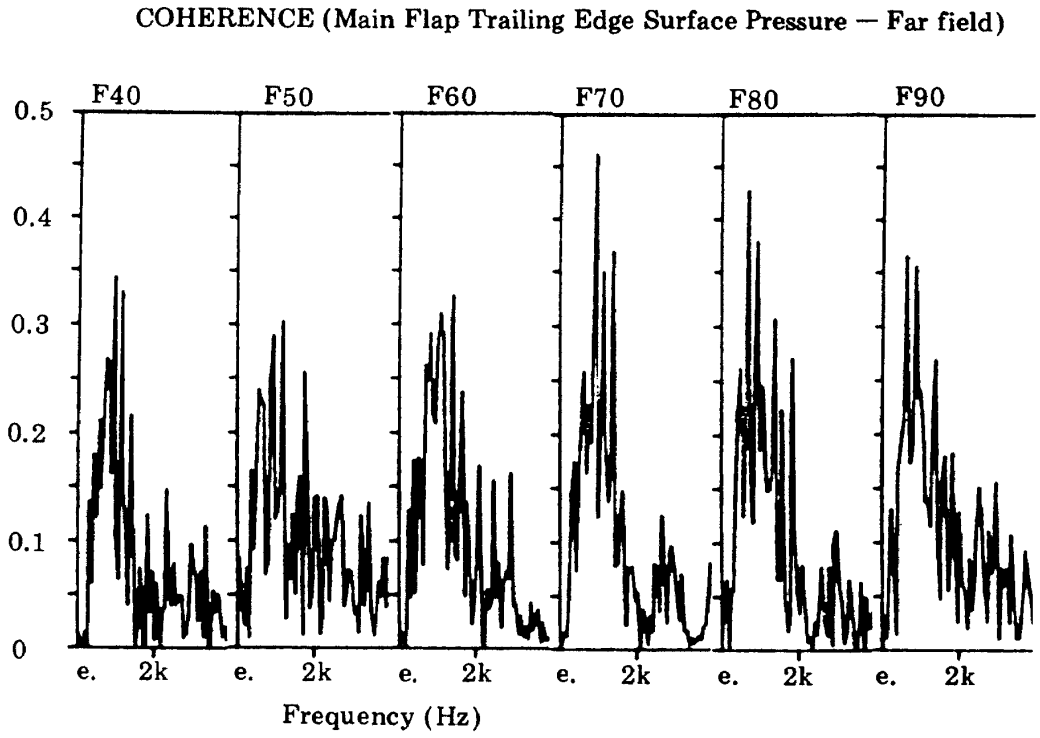

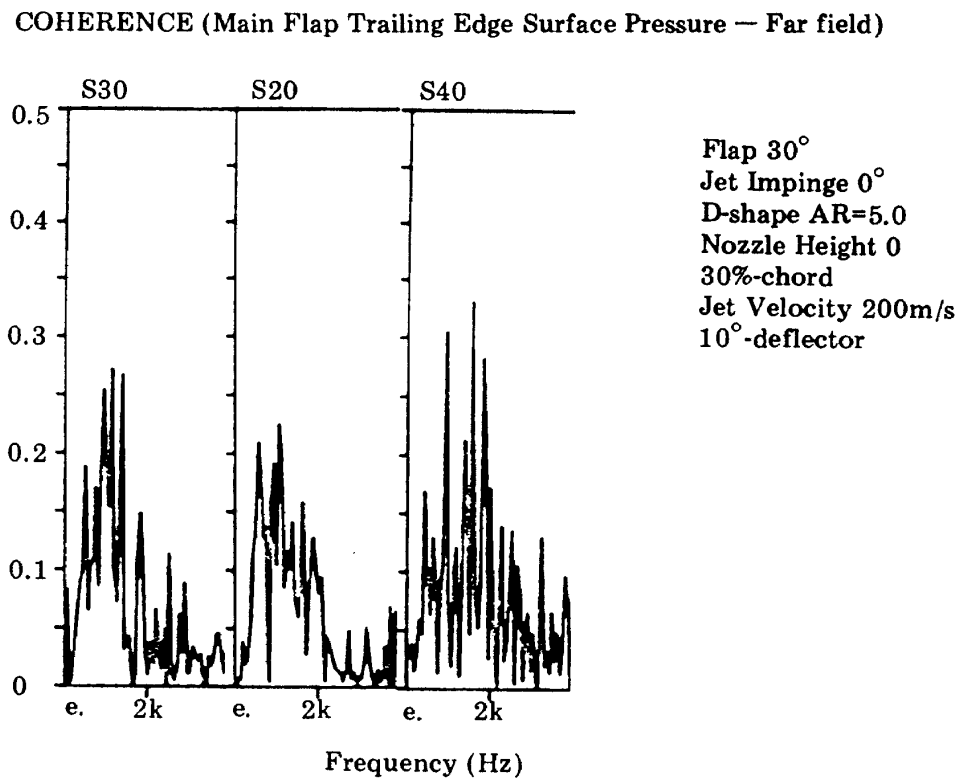

Figure 16 Coherence across flap trailing edge surface pressure at jet velocity 200m/s

Frequency ranges at peak coherence are found to be the same ranges as in the far-field noise spectra from USB-PHLS when they were taken at the flap trailing edge; also for these frequency ranges, the flap trailing edge was the highest magnitude of coherence location.

From these results hitherto, it could be concluded that the flap trailing edge is the most predominant noise source

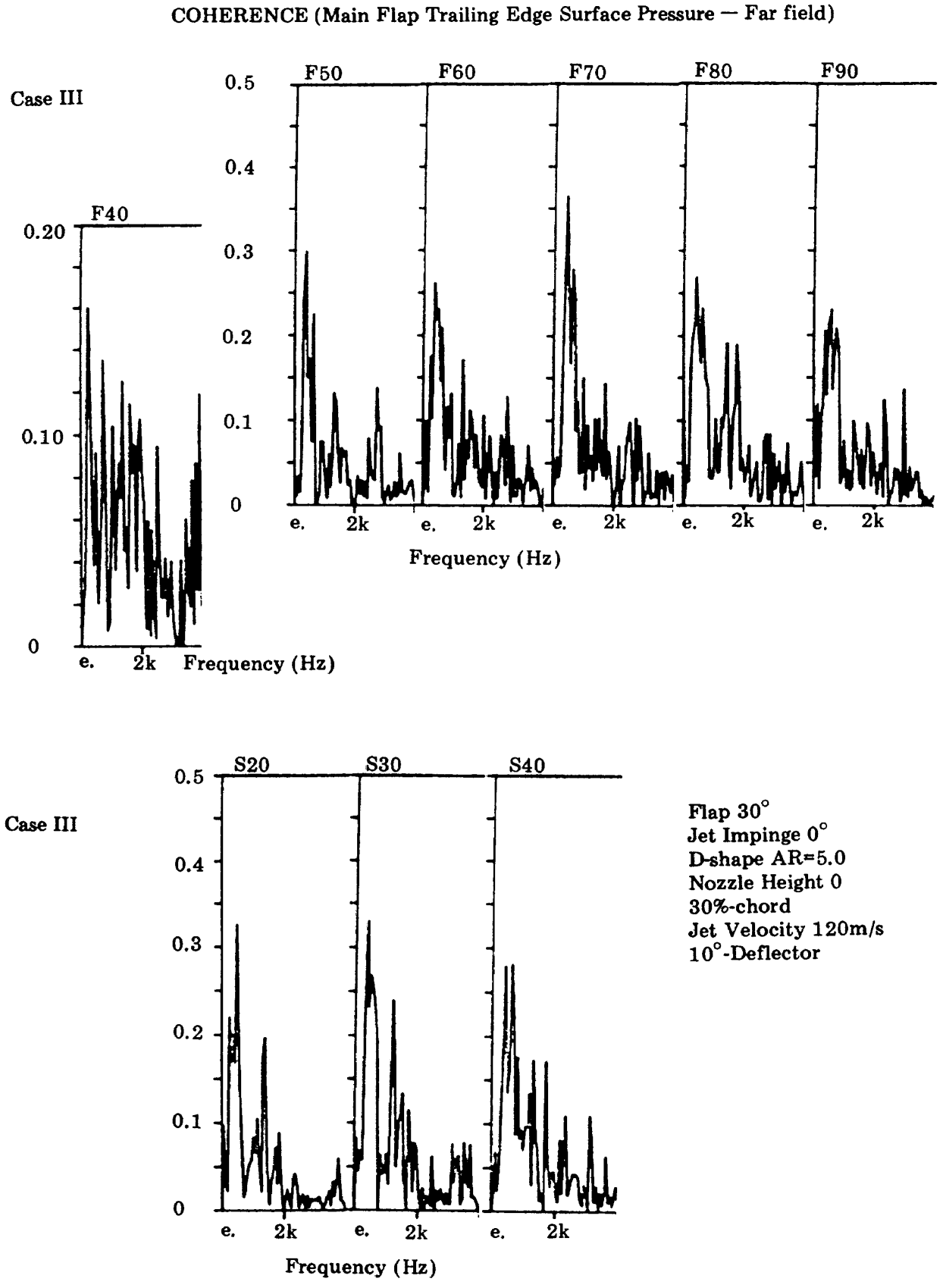

Figure 17 Coherence across flap trailing edge surface pressure at jet velocity 120m/s

and is contributive to frequency ranges of peak sound intensity level in the far-field spectrum of USB-PHLS system noise.

USB-PHLS system noise below the wing/flap as the measure of a community noise differs in its fundamental aeroacoustic mechanisms which will depend upon its system configuration geometries. USB-PHLS configuration parameters affect jet flow spreading and attachment characteristics on the wing/flap surface. From the corresponding data of flow visualizations to noise measurements, we have attempted to quantity the jet flow spreading and attachmnent characteristics and to compare them with noise data.

Some flow visualization photographs are shown in Figures 18. For example, Figure 18-2 presents the effect of deflector on jet exhaust flow characteristics over the wing and USB flap, visualized by the Oil Flow method. Without any deflectors (commented as No-deflector in the Figure), the flow is separated near USB main flap. The steeper deflector angles result in better jet flow spreading and thinner wall jet thickness. (cf., Schlieren photograph of 18-3) The exact patterns corresponding to Figure 18-2 are visualized by using the Liquid Crystals (cf., Figure 18-1) which is quick-and-easy visualization method.

Figures 18-4, 18-5 and 18-6 present the effects of the USB nozzle exit shape, the nozzle location relative to the wing, and the jet impingement angle and/or

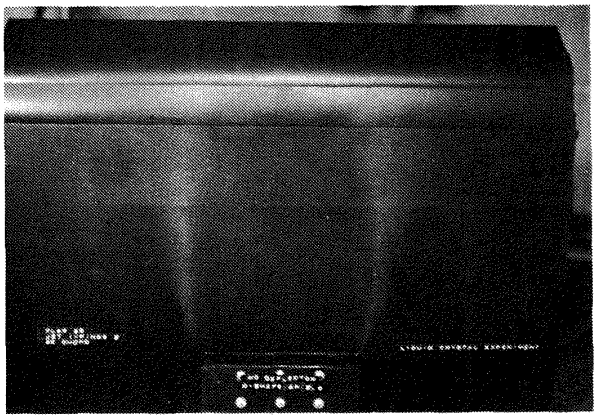

No-deflector 101.5dB (OASPL)
90.6dB (1000Hz)

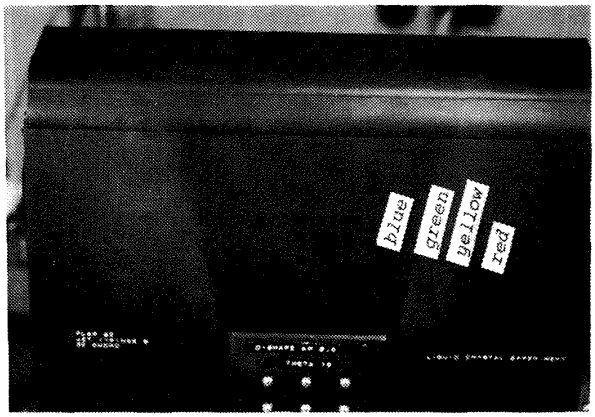

10°-deflector 105.0dB (OASPL)
90.3dB (1000Hz)

0°-deflector

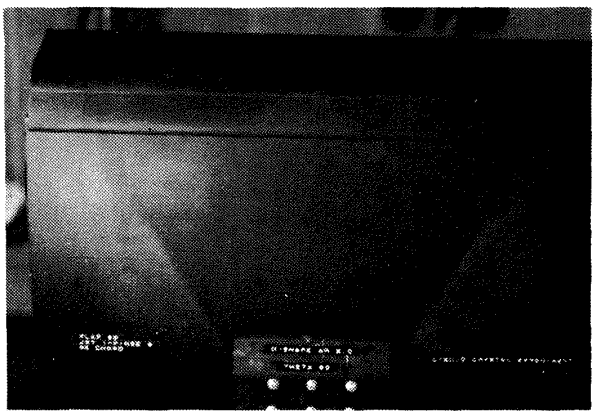

20°-deflector

Figure 18-1 Flow visualization photographs by Liquid Crystals (Effect of Deflector type)
Flap 60°, Jet impinge 6°, 30% chord, 0 nozzle height, jet speed 200m/s, D-shape nozzle AR=5.0

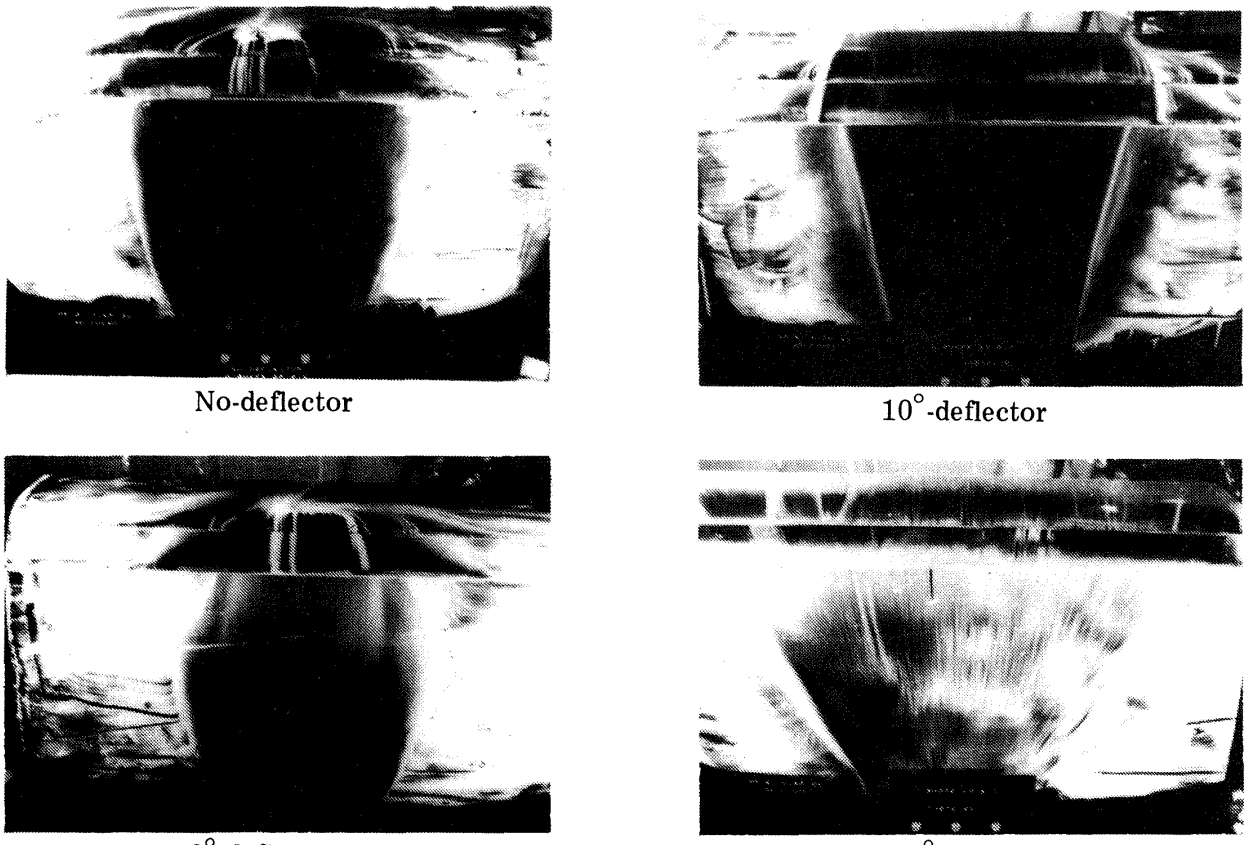

No-deflector　　10°-deflector

0°-deflector　　20°-deflector

Figure 18-2 Flow visualization photographs by oil flows (Effect of Deflector type)
Design parameters were the same as commented in Figure 18-1

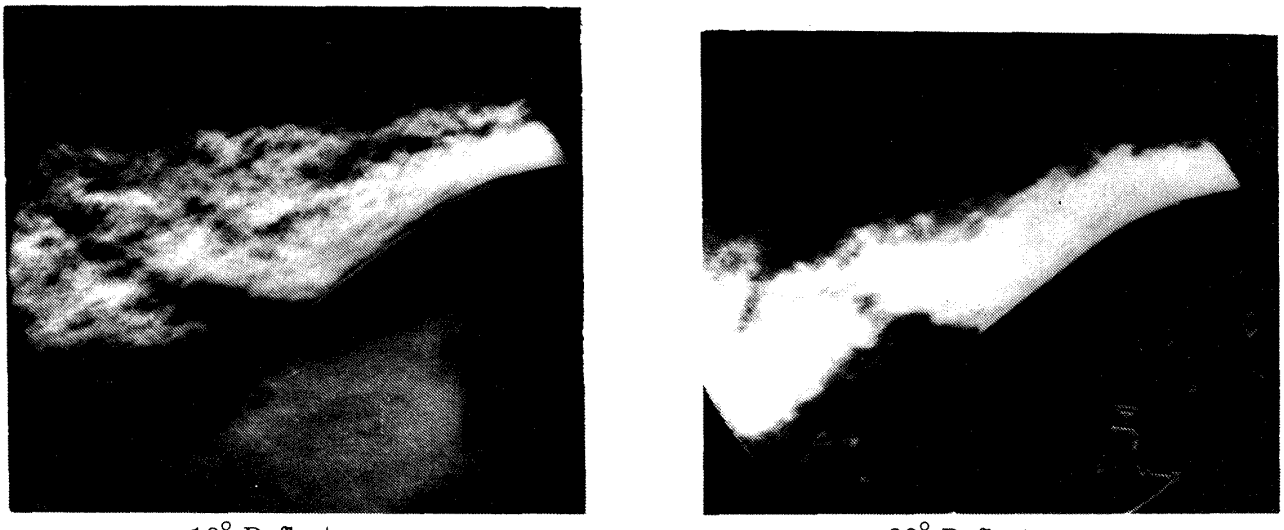

10° Deflector　　20° Deflector

Figure 18-3 Flow visualization photographs by Schlieren (effect of deflector)
6° jet impingement angle, 30° flap setting, Jet velocity 60m/s

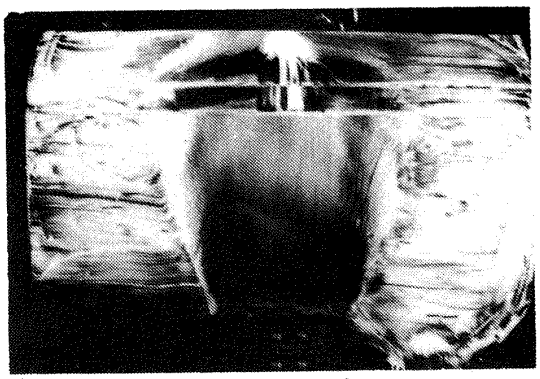

D-shape AR=3.0, No-deflector
103.2dB (OASPL), 94.6dB (1000Hz)

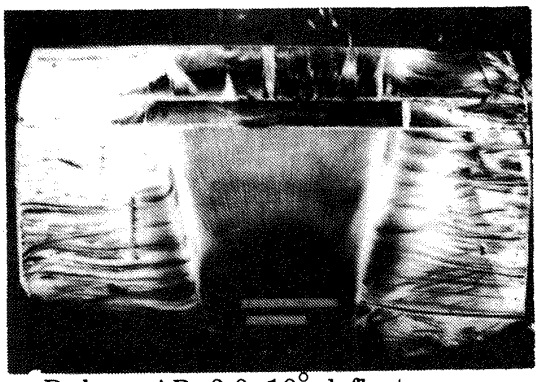

D-shape AR=3.0, 10°-deflector
106.3dB (OASPL), 98.1dB (1000Hz)

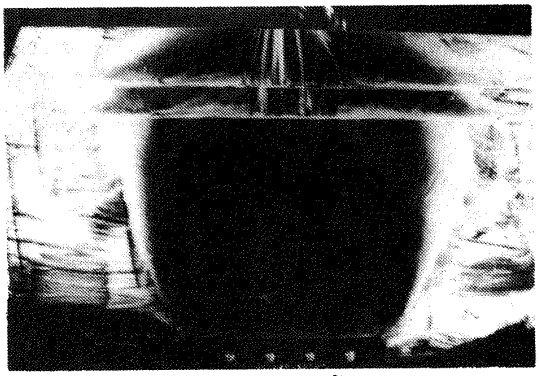

D-shape AR=7.5, No-deflector
103.6dB (OASPL), 94.6dB (1000Hz)

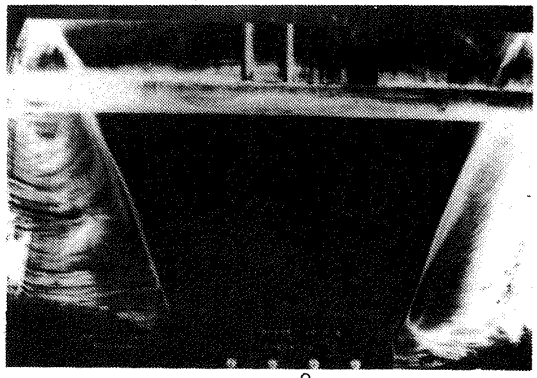

D-shape AR=7.5, 10°-deflector
103.1dB (OASPL), 92.3dB (1000Hz)

Figure 18-4 Flow visualization photographs by oil flow (Effect of Nozzle Shape)
11° jet impinge, 30% chord, 0 nozzle height, 30° flap setting, jet velocity 200m/s

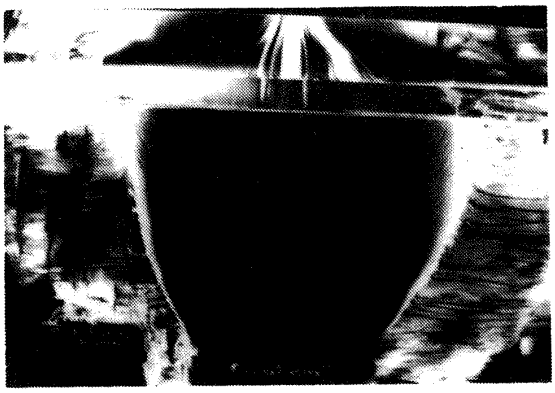

30% chord, no-deflector
104.7dB (OASPL), 96.5dB (1000Hz)

50% chord, no-deflector
103.0dB (OASPL), 96.2dB (1000Hz)

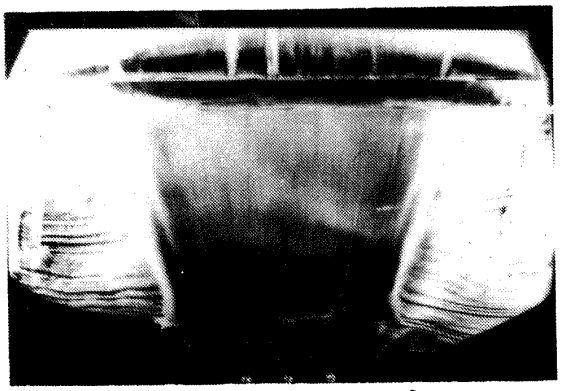

24% chord, 7 nozzle height 10°-deflector
104.6dB (OASPL), 94.7dB (1000Hz)

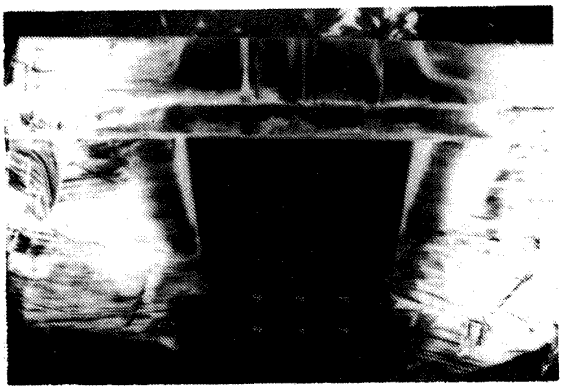

50% chord, 10°-deflector
107.3dB (OASPL), 99.4dB (1000Hz)

Figure 18-5 Flow Visualization photographs by oil flow (effect of nozzle location)
11° jet impinge, D-shape nozzle AR = 5.0, 30° flap setting, 0 nozzle height, Jet velocity 200m/s

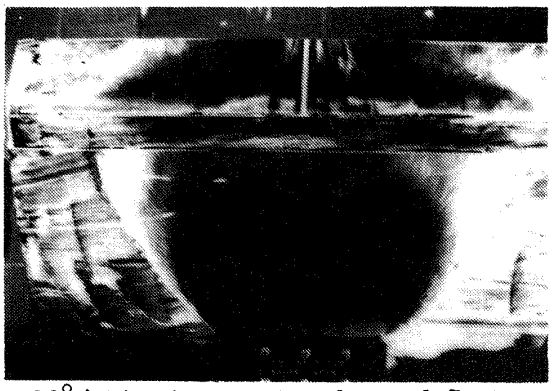

26° jet impingement angle, no-deflector
106.9dB (OASPL), 100.9dB (1000Hz)

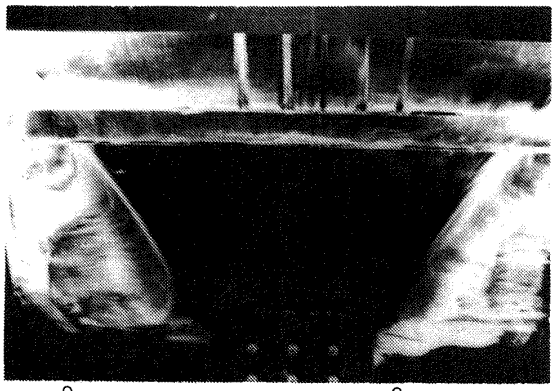

26° jet impingement angle, 0°-deflector

16° jet impingement angle, 10°-deflector
104.3dB (OASPL), 95.1dB (1000Hz)

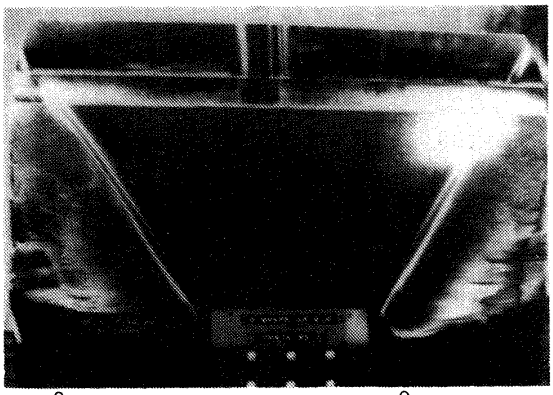

6° jet impingement angle, 20° deflector
103.1dB (OASPL), 92.5dB (1000Hz)

Figure 18-6 Flow visualization photographs by oil flow
(effect of jet impingement angle and deflector angle)
30° flap setting, 30% chord, 0 nozzle height, D-shape nozzle AR=5.0, jet velocity 200m/s

deflector angle respectively. These explanations are given in later paragraphs.

Based on noise and flow visualization data, we introduced the Jet Flow Spreading Parameter $\alpha_{s.p.}$ which is defined as the sum of the attached flow length along the wing/flap surface L_f, jet spreading width (spanwise) at vane X_{vane} and at the main flap trailing edge $X_{t.e.}$ (if totally separated here $X_{t.e.}=0$) divided by the thickness of jet flow at the nozzle exit, h as illustrated in the Figure 19.

Overall sound pressure level from USB-PHLS system measured at the direction below the wing (PHLS-OASPL in abbreviation) for dependence on Jet Flow Spreading Parameter $\alpha_{s.p.}$ is shown in Figure 17. (The Coanda attachment principle implies that $\alpha_{s.p.}$ be drastically parallel to the Jet Turning Angle.)

The general conclusion obtained is that the better jet flow spreading, the lower PHLS-OASPL for sufficiently attached cases, using such as flow deflectors, (where $\alpha_{s.p.}$ greater than 20). The qualitative explanation of Figure 20's result is that, when jet flow is extensively spreading and attached, the turbulence level at the flap trailing edge is eased (cf. Figure 24) due to the mixing and decay process with thinned wall jet thickness (cf. Schlieren photograph of Figure 18-3), so that edge noise is weakened and PHLS noise dominated by edge noise is attenuated. The opposite tendency occurs when jet flow is sepa-

LOSS	GAIN
Coanda Effect-Radiating Sound Deflection to the measuring point below Wing	
Jet Impingement Noise, Jet Scrubbing Noise	Wing/Flap Noise Shielding Effect
Jet-Interacted Edge Noise amplifies to a certain extent (Jet Flow Spreading parameter $\alpha_{s.p.}$ near 20)	Edge Noise attenuation by Jet Spreading, mixing and decay at the Flap Trailing Edge (over $\alpha_{s.p.}$ 20)

USB-PHLS noise reduction trade-off

rated on the wing/flap. The jet flow/edge interaction being very weak, USB-PHLS noise is reduced because of reduced edge-interacted noise; moreover, the wing/flap surface acts as a shield from jet noise and there is no radiating sound deflection to the point below the wing with the Coanda turning. This process is shown in Figure 20 for the case with no-deflector and the parameter $\alpha_{s.p.}$ less than 20.

Next we consider how USB-PHLS congiruation (parameters) affect PHLS-OASPL and the Jet Flow Spreading Parameter $\alpha_{s.p.}$. The effect of variations of jet nozzle exit shape on PHLS-OASPL and jet flow characteristics dependence is shown in Figure 21. The higher aspect ratio (AR in abbreviation) nozzle with deflector results in better jet flow spreading and attachment on the flaps and a lower PHLS-OASPL. The peak PSL frequency-band ranges in the noise spectra shift to higher frequency ranges due to thinned wall jet

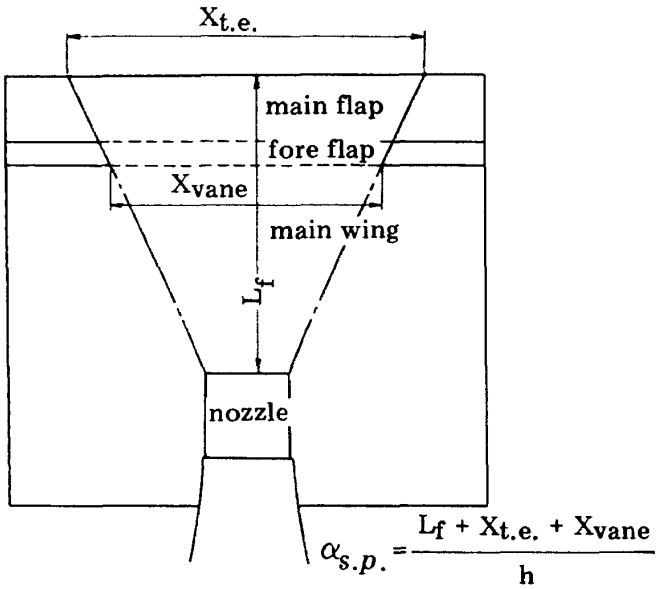

JET FLOW SPREADING PARAMETER

Figure 19 Adefinition of the jet flow spreading parameter $\alpha_{s.p.}$

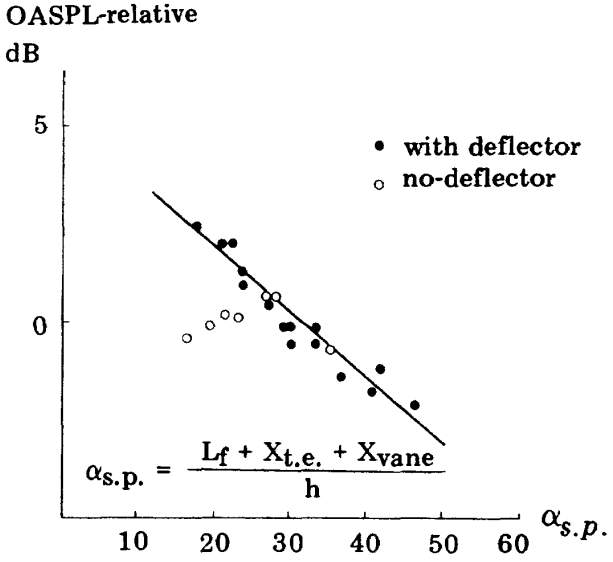

JET FLOW SPREADING PARAMETER DEFINED AS:

Figure 20 OASPL dependence on the jet flow spreading parameter $\alpha_{s.p.}$

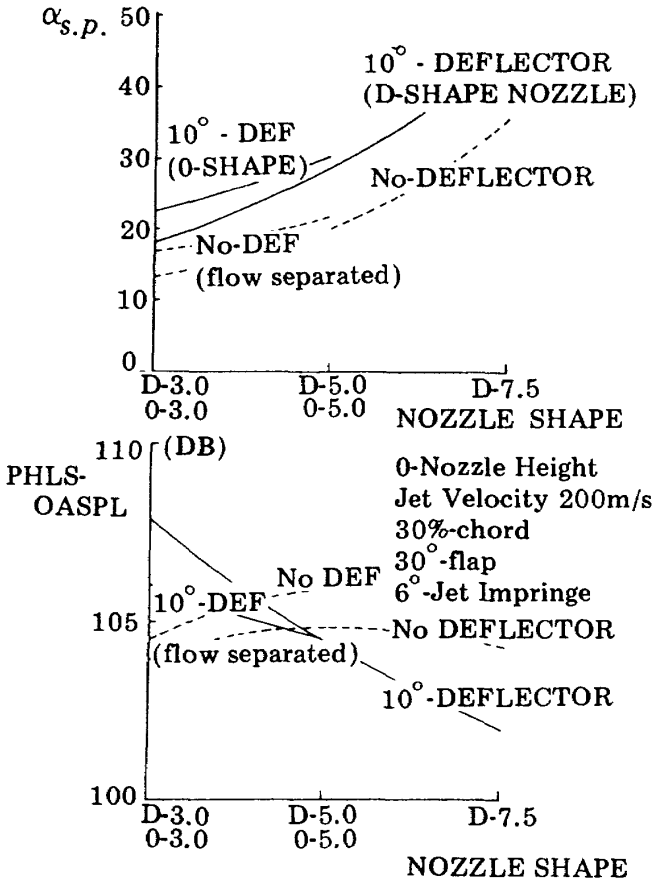

Figure 21 The effect of nozzle exit shape on PHLS-OASPL and the parameter $\alpha_{s.p.}$

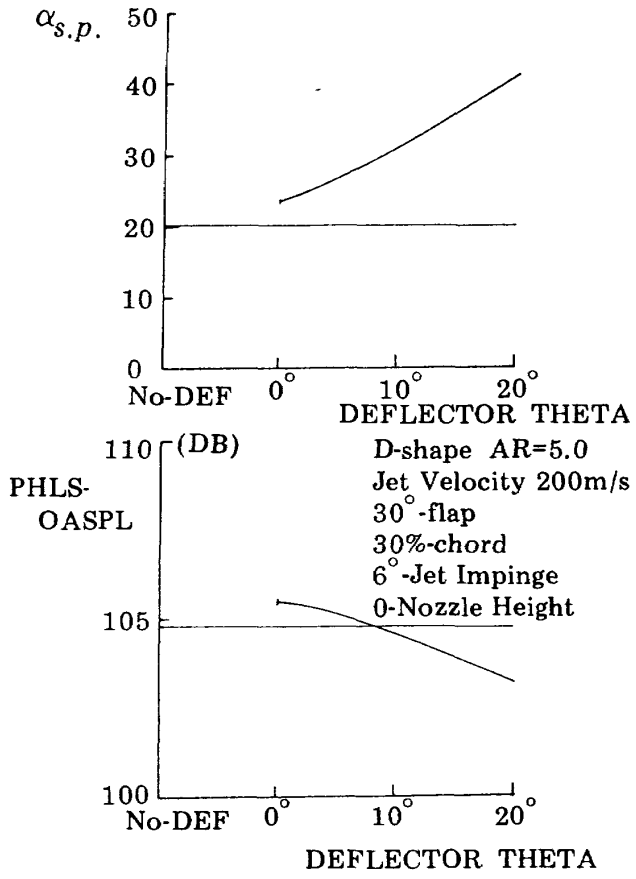

Figure 22 The effect of deflector angle variation on PHLS-OASPL and the parameter $\alpha_{s.p.}$

thickness. The effect of nozzle type on the noise directivity was found to be neglibible.

Exhaust jet flow spreading and attachment characteristics and PHLS-OASPL noise are very sensitive to variations of the deflector angle of theta and the jet impingement angle as shown in Figures 22 and 23. A deflector with no theta angle does not play the role of flow attachment device when the jet impingement angle is small. PHLS-OASPL noise is reduced and the spectrum peak SPL frequency-band is shifted to higher ranges due to the extensive jet flow spreading and mixing decay process which reduces the turbulence level at the flap trailing edge (cf. Figure 24)[6], when the deflector theta angle is sufficiently large.

The similar pattern was found for the jet impingement angle variations.

Figure 25 shows the dependence on the jet nozzle location chordwise. Moving the location from aft (50% chord in Figure 25) to forward chordwise location (24% chord), a tendency toward better flow attachment is found which again results in reduced PHLS-OASPL.

As for the parameter of jet nozzle height location, the nozzle adjacent to the main wing surface is better optimized. And also noise shielding for lower part of aft quadrant directions is more effective for forward chordwise locations and the low nozzle height locations.

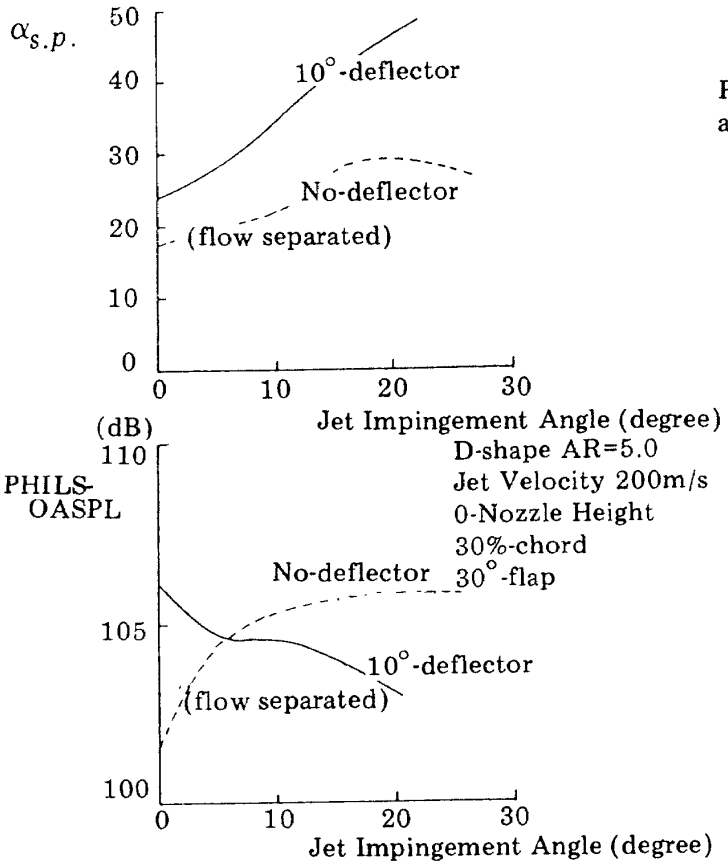

Figure 23 The effect of jet impingement angle variation on PHILS-OASPL and $\alpha_{s.p.}$

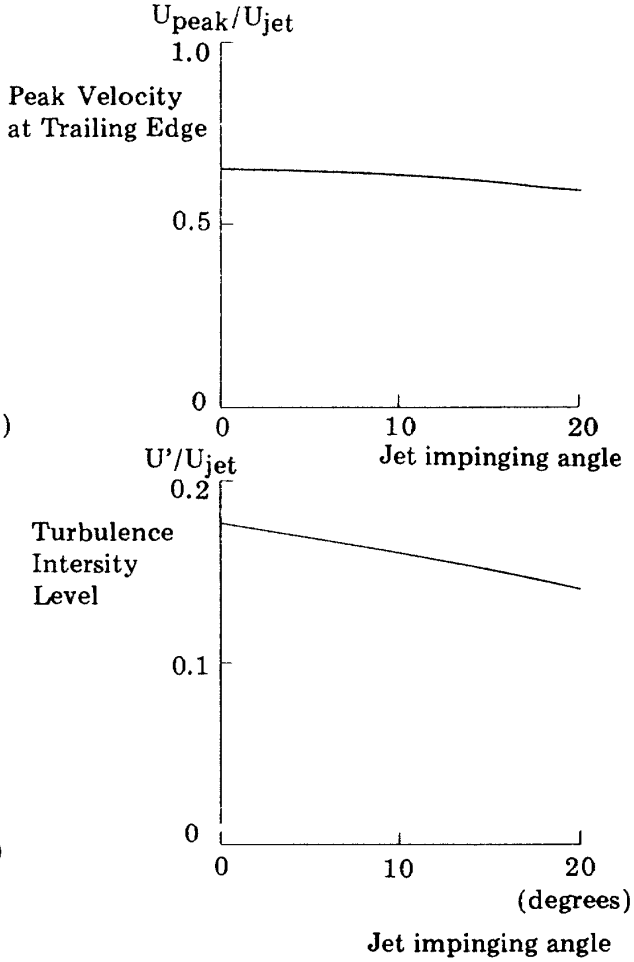

Figure 24 The effect of jet impingement angle variation on peak velocity and turbulence intensity level at flap trailing edge

It was concluded that the trailing edge noise is the most predominant noise source of USB-PHLS configuration from a community noise view point. We next refer to this edge noise attenuation techniques. Based upon the preceding data and the morphology of past studies, it can be suggested that the edge noise attenuation is accomplished by the following mechanisms:

Modifying the turbulence flow field in the vicinity of the flap trailing edge by edge designs such as irregular or serrated designs which weaken the shear-layer velocity gradients and turbulence amplification near the edge (Serrated edge designs was suggested by Allan and Hayden[7]);

Controlling edge impedance and absorbing noise or turbulence energy by acoustically treated flap edges.

Figure 26 shows the treated main flap trailing edges, i.e., perforated metal flap with metal wool fillings, porous flap and serrated edge designs being compared with the conventional solid flap.

Applying these attenuation techniques, noise reduction data were obtained. As an example, Figure 27 shows noise reduction by perforated flaps. Further attempt to optimize the metal porousity or pitches would result in

more efficient noise reductions. Acoustically treated flaps were thought to have a potential to reduce more than 6dB at the peak SPL frequency-bands.

Modifying the turbulence flow field in the vicinity of the edge by slit secondary blowing flap (cf., Figure 28-1), we have obtained noise reduction data as shown in Figure 28-2. The secondary blowing flap concept is thought to be effective as well for improving exhaust jet turning characteristics as a jet flap. However taking into account the structure penelties such as ducting system for secondary air bleeds from engine compressors, 5dB reduction at peak frequency-bands might not be effective.

By having a slot between the wing and USB flap (cf., Figure 29-1), induced air from a slot modifies the flow field over flap trailing edge portions. Slot width dependence on PHLS noise is presented in Figure 29-2. This concept would result in thrust augmentation by induced

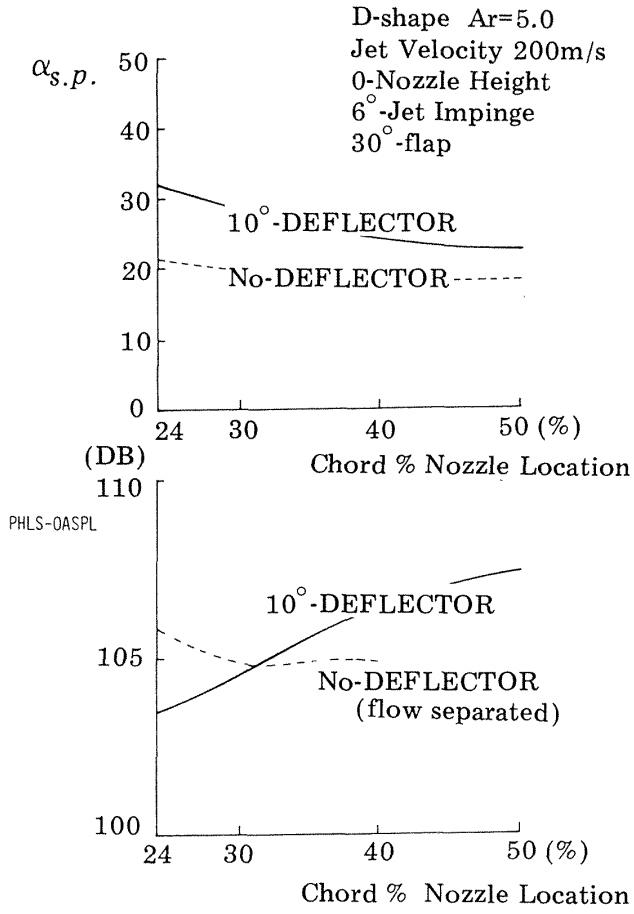

Figure 25 The effect of chordwise locations of USB nozzle on PHLS-OASPL and the parameter $a_{s.p.}$

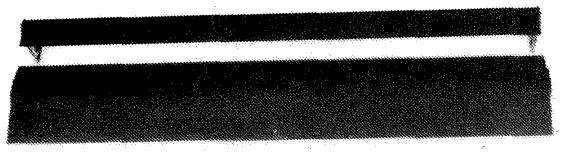

Solid flap as baseline

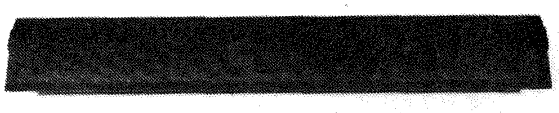

Perforated flap

Porous flap

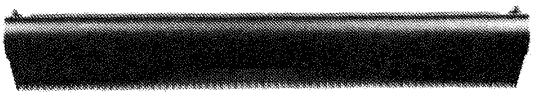

Serrated flap

Figure 26 Photographs of treated main flap

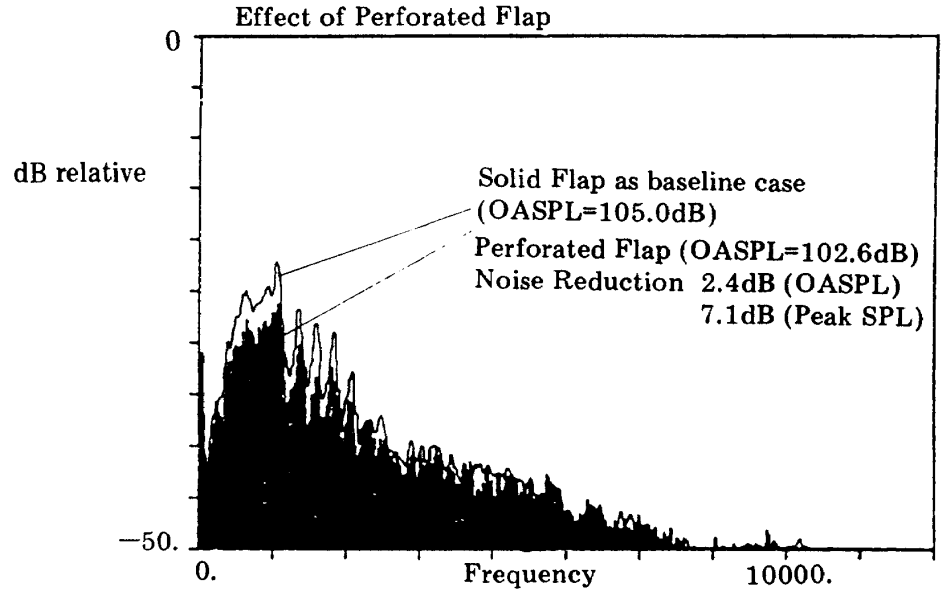

Figure 27-1 PHLS-OASPL noise reduction by perforated flap
(Narrow-band SPL analysis up to 10000Hz)

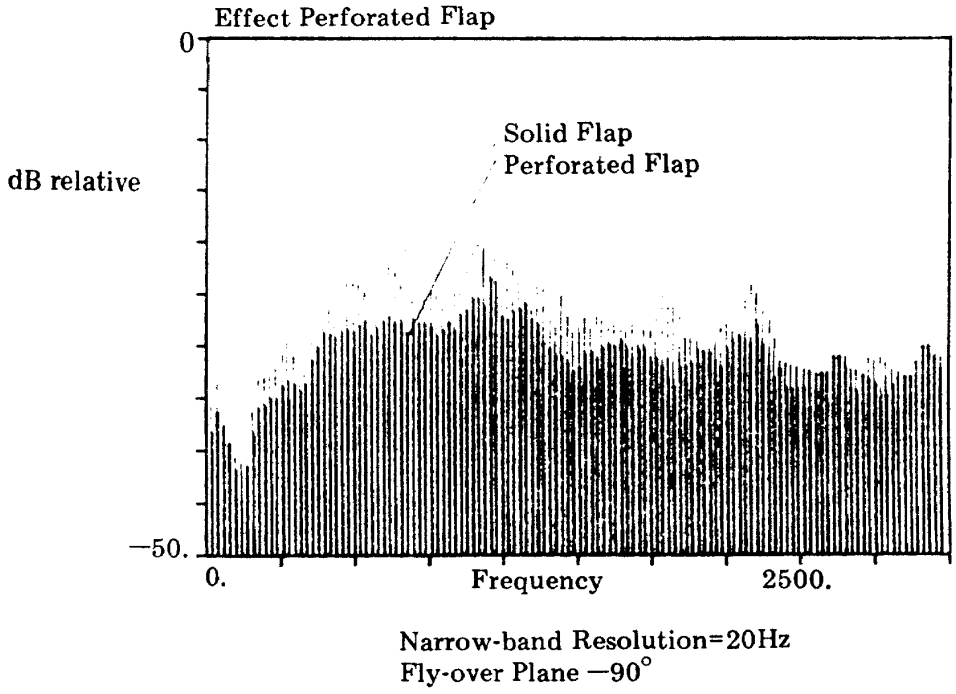

Figure 27-2 PHLS-OASPL noise reduction by perforated flap
(Narrow-band SPL analysis up to 2500Hz)

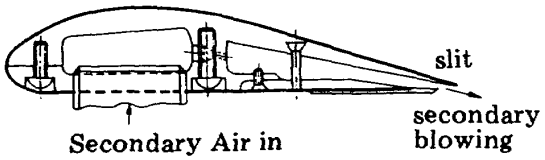

SECONDARY BLOWING FLAP

Figure 28-1 A section of secondary blowing flap slit width being variable by slit plate spanwise length of slit blowing is 360mm

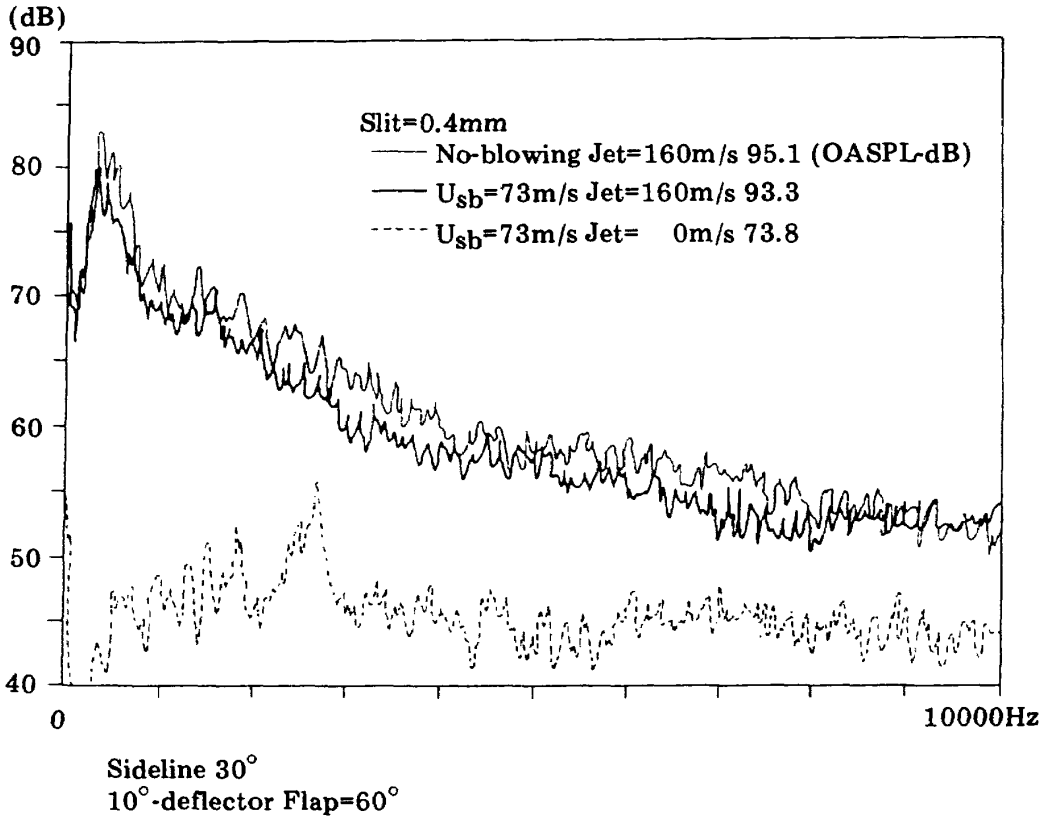

Figure 28-2 PHLS noise reduction by slit secondary blowing flap in narrow-band spectra

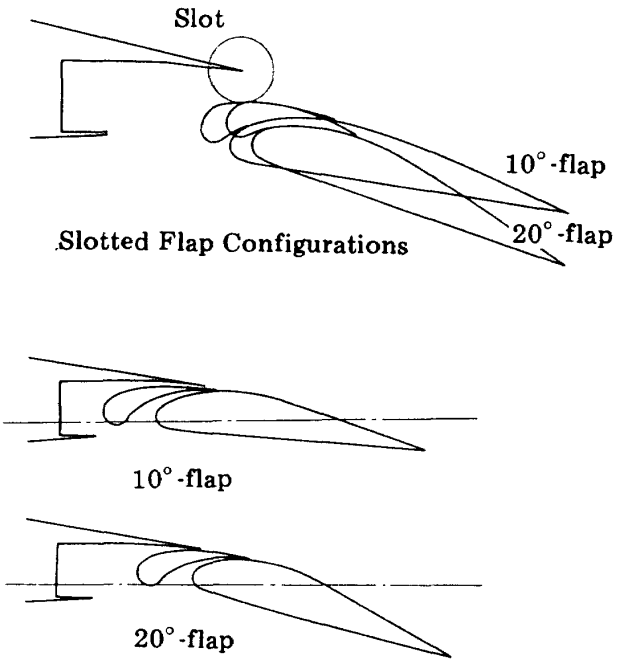

Figure 29-1 Slotted flap configuration being compared with basic double flap configurations (slot is 0.1% flap chord)

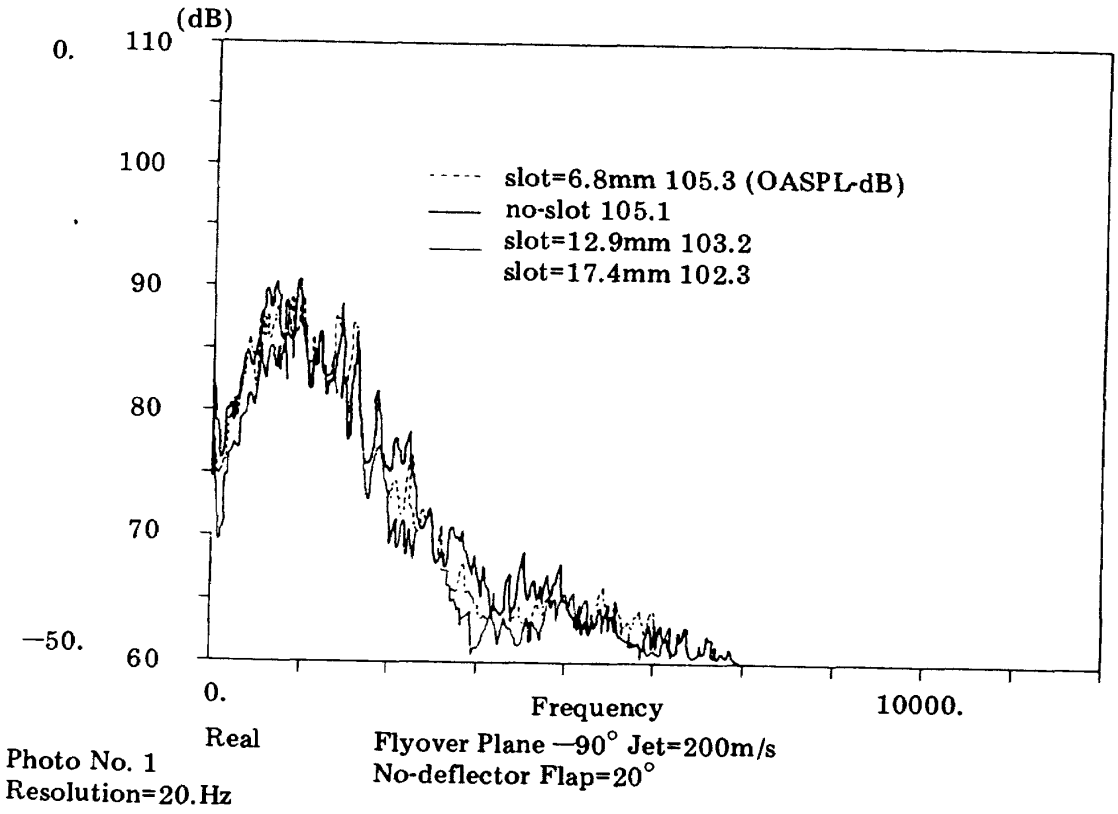

Figure 29-2 PHLS noise reduction by slotted flap

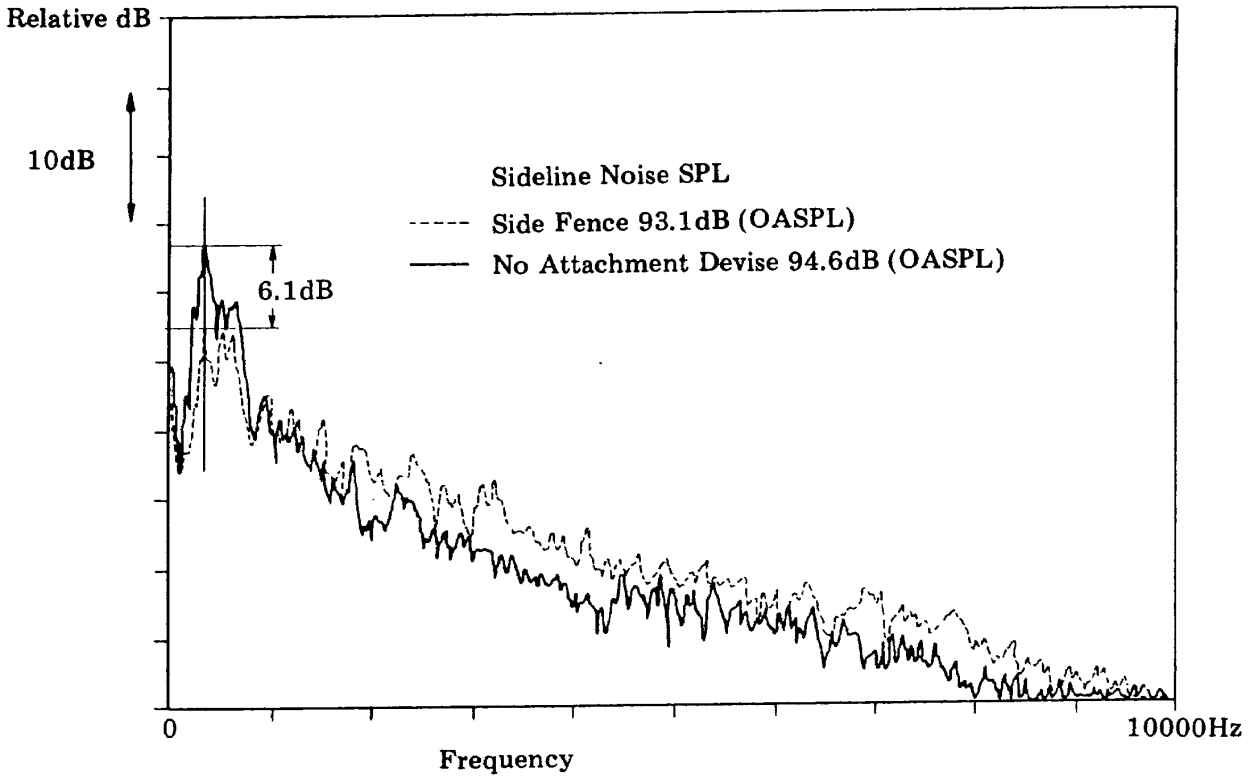

Figure 30 Side line noise reduction by Side Fence

flow from a slot and is effective for takeoff flap configurations[8]. For landing flap configuration δ_f=60° exhaust jet tends to be separated by a slot and hence deteriorating aerodynamic performances.

For a certain case that vortex motions of exhaust jet flow near side edges of flap generating noise which then influencing PHLS noise at a Sideline direction, installing Side fences[9] suppresses these source of noise by changing sideline mixing processes. In Figure 30, noise reduction by Side Fence at the sideline direction is presented.

CONCLUDING REMARKS

The acoustic characteristics of the external upper surface blowing concept of powered high lift systems are studied experimentally using 8%-scale cold flow model, together with the visualization of corresponding exhaust jet flow characteristics on wing/flap surface. The main conclusions are summarized as follows:

[1] Exhaust jet velocity exponents of radiating sound intensity level from upper surface blowing PHLS configuration varies as $U_{jet}^{5.1}$ — $U_{jet}^{5.9}$ depending on the direction.

[2] Estimated Strouhal number, corresponding to the peak intensity level frequency in the normalized SPL spectral density, takes approximately the same value of 0.05.

[3] The flap trailing edge noise is the predominant noise source of USB-PHLS configuration at the direction

below the wing/flap.

[4] By introducing the jet flow spreading parameter $\alpha_{s.p.}$, exhaust jet flow characteristics are related to the acoustic characteristics—i.e., the better jet flow spreading and attachment, the lower the PHLS-OASPL for practical attached flow cases.

[5] Noise reduction data were obtained by optimizing the basic USB-PHLS structural geometries for the lowest noise, among which, the jet nozzle location relative to wing/flap and nozzle exit shape, and the flow attachment device are important parameters.

[6] Several noise reduction techniques using acoustically treated flaps, slot secondary blowing flap and serrated trailing edge design were applied to attenuate the edge noise, and throught to have the potential to reduce more than 6dB at the peak SPL frequency-bands.

[7] The installation of side fences suppresses flap side edge generated noise.

Acknowledgement

These researches were carried out as a part of the Fanjet STOL Aircraft Research Project initiated by National Aerospace Laboratory. The authors would like to express sincere thanks to the Divisions Directors, Mr. Tadao Torisaki and Dr. Masakatsu Matsuki, for their valuable advices and comments.

REFERENCE

(1) Reddy, N.N., et. al., NSAS SP-406, 1976

(2) Brown, W.H., Lockheed-Georgia Engineering Report LG74-0127, 1974

(3) Tam. C.K., J. of Acoustic Soc. America, vol. 57, 1975

(4) Ffowcs Williams, J.E., J. of Fluid Mech., vol. 40, 4, 1970

(5) Hayden, R.E., NASA CR-2126, 1972

(6) Brown, W.H. and Reddy, N.N., NASA SP-406, 1976

(7) Hayden, R.E., AIAA Paper 76-500 and NASA CR-112166, 1976

(8) Miyashita, J., KAMPF T/O Flap Wind Tunnel Experiments Data Kawasaki Heavy Industries Rep. STOL 52-146, 1977.

(9) Maita, M. et. al., ASME/AIAA Paper 80—1244, 1980
Maita, M. et. al., Journal of Aircraft, Vol.19, No.3, 1981.

TECHNICAL REPORT OF NATIONAL
AEROSPACE LABORATORY
TR-685T

航空宇宙技術研究所報告685T号(欧文)

昭和56年10月発行

発行所　航空宇宙技術研究所
東京都調布市深大寺町1,880
電話 武蔵野三鷹(0422)47-5911(大代表)
印刷所　株式会社　実業公報社
東京都千代田区九段南4-2-12

Published by
NATIONAL AEROSPACE LABORATORY
1,880 Jindaiji, Chofu, Tokyo
JAPAN